CELL BIOLOGY

Mitophagy restricts BAX/BAK-independent, Parkin-mediated apoptosis

Giovanni Quarato[1]†‡, Luigi Mari[1]†, Nicholas J. Barrows[2]§, Mao Yang[1], Sebastian Ruehl[1]||, Mark J. Chen[1]¶, Cliff S. Guy[1], Jonathan Low[2], Taosheng Chen[2], Douglas R. Green[1]*

Degradation of defective mitochondria is an essential process to maintain cellular homeostasis and it is strictly regulated by the ubiquitin-proteasome system (UPS) and lysosomal activities. Here, using genome-wide CRISPR and small interference RNA screens, we identified a critical contribution of the lysosomal system in controlling aberrant induction of apoptosis following mitochondrial damage. After treatment with mitochondrial toxins, activation of the PINK1-Parkin axis triggered a BAX- and BAK-independent process of cytochrome c release from mitochondria followed by APAF1 and caspase 9–dependent apoptosis. This phenomenon was mediated by UPS-dependent outer mitochondrial membrane (OMM) degradation and was reversed using proteasome inhibitors. We found that the subsequent recruitment of the autophagy machinery to the OMM protected cells from apoptosis, mediating the lysosomal degradation of dysfunctional mitochondria. Our results underscore a major role of the autophagy machinery in counteracting aberrant noncanonical apoptosis and identified autophagy receptors as key elements in the regulation of this process.

INTRODUCTION

Parkin is an E3 ubiquitin ligase that participates in the processes of proteasomal and lysosomal degradation (*1*). In its autoinhibited inactive state, Parkin is located in the cytosol and, upon mitochondrial impairment, translocates onto mitochondria (*2*), where it shows exquisite specificity for proteins on the outer mitochondrial membrane (OMM) (*3*); ubiquitination of which is considered to be the initial step of the complex process termed mitophagy (*3*). This process mediates the degradation of dysfunctional mitochondria to maintain cellular homeostasis. During mitophagy, the protein PTEN-Induced Kinase 1 (PINK1) is required for Parkin activation. Unlike Parkin, PINK1 localizes to the OMM, where it is imported and degraded in healthy mitochondria by mitochondrial proteases (*4*) and released into the cytosol for degradation by the ubiquitin-proteasome system (UPS) (*5*). Mitochondrial membrane depolarization stabilizes PINK1 on the OMM (*4*, *6*) in association with the translocase of the OMM complex (*7*). PINK1 phosphorylates ubiquitin (*8*) and the Parkin ubiquitin-like domain (*9*). This phosphorylation event results in the full activation state of Parkin and its translocation to the OMM (*3*). Here, the E3 ubiquitin ligase function of Parkin ubiquitinates substrates on the OMM, amplifying the signal that recruits both the UPS (*10*–*13*) and a small class of cytosolic proteins, the autophagy receptors, to the damaged mitochondrion. These receptors contain a microtubule-associated protein 1A/1B light chain 3 (LC3)–interacting region (LIR) domain that recruits members of the autophagy related 8 (ATG8) family (*14*), finally giving rise to the formation of autophagosomes around mitochondrial remnants and their fusion with lysosomes (*11*–*13*).

Mutations in both *PRKN* and *PINK1*, encoding Parkin and PINK1, respectively, are associated with genetic forms of early-onset Parkinson's disease (PD) (*15*, *16*). Because both PINK1 and Parkin are required for mitochondrial homeostasis (*17*, *18*) and regulate mitophagy (*19*, *20*), it is thought that dysfunction in mitophagy can cause PD, suggesting that the accumulation of dysfunctional mitochondria may induce loss of neuronal function and eventually cell death (*20*). *PRKN* mutations and loss of heterozygosity have also been observed in different types of cancer (*21*). In a landscape of somatic copy number alterations across human cancer, Parkin is one of the most deleted genes, therefore considered a tumor suppressor.

Other possible mechanisms, such as escape from cell death, can drive the process of tumorigenesis (*22*). A specific link between PINK1 and Parkin activity to promote cell death has been suggested by several studies (*23*–*26*). A type of autophagy-dependent cell death that could explain the onset of cell death in the context of aberrant intracellular catabolic processes such as mitophagy has been previously described (*27*, *28*), but the mechanism of action remains elusive, and the interpretation of this phenomenon is controversial (*29*).

We therefore sought to reassess the role of Parkin in cell death. Using in vitro and in vivo models as well as two different whole-genome screening approaches, we report that Parkin expression sensitized cells to die and that this process required the kinase activity of PINK1 and the degradation activity of the UPS. This process of cell death was independent of the B cell lymphoma 2 (Bcl2) family members but involved caspase activation mediated by assembly of the apoptosome. We found that Parkin-dependent cytochrome c (cyt c) release from the intermembrane space was mediated by UPS activity on the OMM and that lysosomal degradation of mitochondrial remnants was protected from cell death. Last, we identified the recognition of ubiquitinated OMM proteins by

[1]Department of Immunology, St. Jude Children's Research Hospital, Memphis, TN 38105, USA. [2]Department of Chemical Biology and Therapeutics, St. Jude Children's Research Hospital, Memphis, TN 38105, USA.
*Corresponding author. Email: douglas.green@stjude.org
†These authors contributed equally to this work.
‡Present address: Treeline Biosciences, San Diego, CA 92121, USA.
§Present address: GSK, Rockville, MD 20850, USA.
||Present address: T3 Pharmaceuticals AG, Allschwil 4123, Switzerland.
¶Present address: Department of Laboratory Medicine, Cleveland Clinic, Cleveland, OH 44195, USA.

autophagy receptors as a cell fate decision point downstream the activation of the PINK1-Parkin axis.

RESULTS

Parkin sensitizes cells to apoptosis in a PINK1-dependent manner

To ask whether Parkin plays a role in regulating cell death, immortalized mouse embryonic fibroblasts (MEFs) stably expressing yellow fluorescent protein–Parkin (YFP-Parkin MEFs) (fig. S1A) were treated with chemical compounds that induce mitochondrial depolarization, e.g., valinomycin or the combination of antimycin A and oligomycin. As expected, both treatments rapidly dissipated the mitochondrial transmembrane potential, as detected by the potentiometric dye tetramethylrhodamine ethyl ester perchlorate (TMRE) (fig. S1B), and increased mitochondrial reactive oxygen species production, as assessed using the Mitochondrial Superoxide Indicator (MitoSOX) (fig. S1C). Consistent with previous reports (*2*, *6*, *30*), chemically induced mitochondrial uncoupling triggered mitophagy in YFP-Parkin MEFs, as depicted by the pH-sensitive mitochondrial probe mitochondrial mKeima (mt-mKeima) that visualizes the delivery of impaired mitochondria to lysosomes (fig. S1, D and E). Treatment of YFP-Parkin MEFs with these mitochondrial agents resulted in cell death as assessed by propidium iodide (PI) positivity (Fig. 1, A and B). Cotreatment with the pan-caspase inhibitor q-VD-OPh (qVD) delayed cell death, suggesting that cell death occurred by apoptosis, a conclusion supported by the typical apoptotic morphology of YFP-Parkin MEFs treated with valinomycin (Fig. 1, A and B, and fig. S1F). As controls, compounds that induce intrinsic apoptosis, such as actinomycin D, thapsigargin, and tunicamycin were able to induce cell death independently of the expression of Parkin (Fig. 1A). Similar observations were made using the human colon cancer cell line HCT116 (fig. S1, A and G).

To gain additional insights into the effects exerted by valinomycin treatment, we performed a clonogenic survival assay with MEFs expressing YFP-Parkin. Notably, increasing concentrations of valinomycin caused progressive loss of clonogenic survival only in YFP-Parkin MEFs (Fig. 1C). We then took advantage of this observation to perform a genome-wide CRISPR-Cas9 knockout (KO) screen to identify genes that, when ablated, could restore clonogenic survival under our experimental conditions (fig. S1H). Using two different concentrations of valinomycin and three rounds of treatment, we enriched for pools of cells that significantly expressed multiple single guide RNAs (sgRNAs) targeting the same gene. We found and validated that *Pink1* was the only gene whose absence could restore the clonogenic survival of the YFP-Parkin MEFs (Fig. 1, D and E; fig. S1, I and J; and table S1).

To investigate how PINK1 participates in this Parkin-mediated form of cell death, we developed an inducible in vitro system to express a stable, mitochondrial-targeted, and active form of PINK1 (acPINK1) by which Parkin translocation to the OMM is achieved without the use of any mitochondrial uncoupler (*6*). Doxycycline (Dox) induction of acPINK1 induced apoptosis of YFP-Parkin HCT116 cells, as depicted by PI positivity and poly(adenosine diphosphate–ribose) polymerase 1 (PARP) cleavage, which was inhibited by qVD (Fig. 1F and fig. S1K). Moreover, we confirmed a previous report (*6*) showing that expression of acPINK1 triggered mitophagy, as depicted here by the degradation of the mitochondrial protein cyt c oxidase subunit 5B (COX Vb), and this process was not inhibited by qVD. These results indicate that Parkin expression sensitizes cells to apoptosis upon mitochondrial depolarization, and PINK1 is both necessary and sufficient to trigger the cascade of events leading to cell death.

Parkin-mediated apoptosis is a BAX- and BAK-independent mechanism

To further characterize the observed Parkin-mediated form of apoptosis, we ablated in YFP-Parkin MEFs the apoptotic protease activating factor 1 (APAF1), which is the core component of the apoptosome required for the activation of mitochondrial apoptosis (fig. S2A) (*31*). As expected, cells lacking APAF1 were protected from cell death, induced upon treatment with mitochondrial uncouplers, a combination of BH3 mimetics (ABT737 and S63845), or actinomycin D. In contrast, we observed that PINK1 KO cells were only protected from death induced by mitochondrial uncouplers (Fig. 2A). However, while the absence of PINK1 restored clonogenic survival in YFP-Parkin MEFs treated with valinomycin, the absence of APAF1 did not (Fig. 2B). Moreover, in the same cells treated with BH3 mimetics, the absence of PINK1 or APAF1 could not restore clonogenic survival. This suggests that activation of the PINK1-Parkin pathway might trigger a mitochondrial catastrophe that ultimately leads to a caspase-independent form of cell death (*32*).

To further explore this phenomenon, we generated cells lacking the two major proapoptotic Bcl2 effector proteins, the BCL2 associated X apoptosis regulator (BAX) and the BCL2 antagonist/killer 1 (BAK), which are known to be required for mitochondrial outer membrane permeabilization (MOMP), leading to caspase activation and apoptosis (*33*). As expected, YFP-Parkin MEFs or YFP-Parkin HCT116 lacking BAX and BAK ($Bax^{-/-}$ $Bak^{-/-}$) were completely resistant to cell death induced by BH3 mimetics and other conventional inducers of apoptosis (Fig. 2C and figs. S1A and S2B). They remained, however, fully susceptible to cell death induced by raptinal, which is known to bypass BAX and BAK activation (*34*), and by valinomycin or by the combination of antimycin A and oligomycin, suggesting that BAX and BAK are dispensable for this Parkin-dependent cell death (Fig. 2C and figs. S1A and S2B). In line with this observation, $Bax^{-/-}$ $Bak^{-/-}$ YFP-Parkin MEFs exhibited clonogenic survival when treated with a combination of BH3 mimetics but not after treatment with valinomycin (Fig. 2D). Furthermore, the absence of BAX and BAK did not influence the capacity of the cell to undergo mitophagy (fig. S2C).

To further characterize this Parkin-dependent cell death, we assessed MOMP by monitoring mitochondrial cyt c release by flow cytometry analysis of digitonin-permeabilized cells (*35*). $Bax^{-/-}$ $Bak^{-/-}$ YFP-Parkin MEFs treated with valinomycin showed cyt c release from the mitochondria, which, as expected, was not detectable after BH3 mimetics treatment (Fig. 2E). In addition, in the same cells, while this form of cell death was delayed by the CRISPR deletion of either *Apaf1* or caspase 9 (*Casp9*), it was not affected by the enforced expression of the antiapoptotic Bcl2 proteins—BCL2, the BCL2-like 1 (BCL-xL), or the myeloid cell leukemia sequence 1 (MCL1) (Fig. 2, F and G, and fig. S2, D to F). Together, these results imply that the apoptosis-inducing activity of valinomycin in cells expressing Parkin is mediated independently of the activity of the proapoptotic Bcl2 family members BAX and

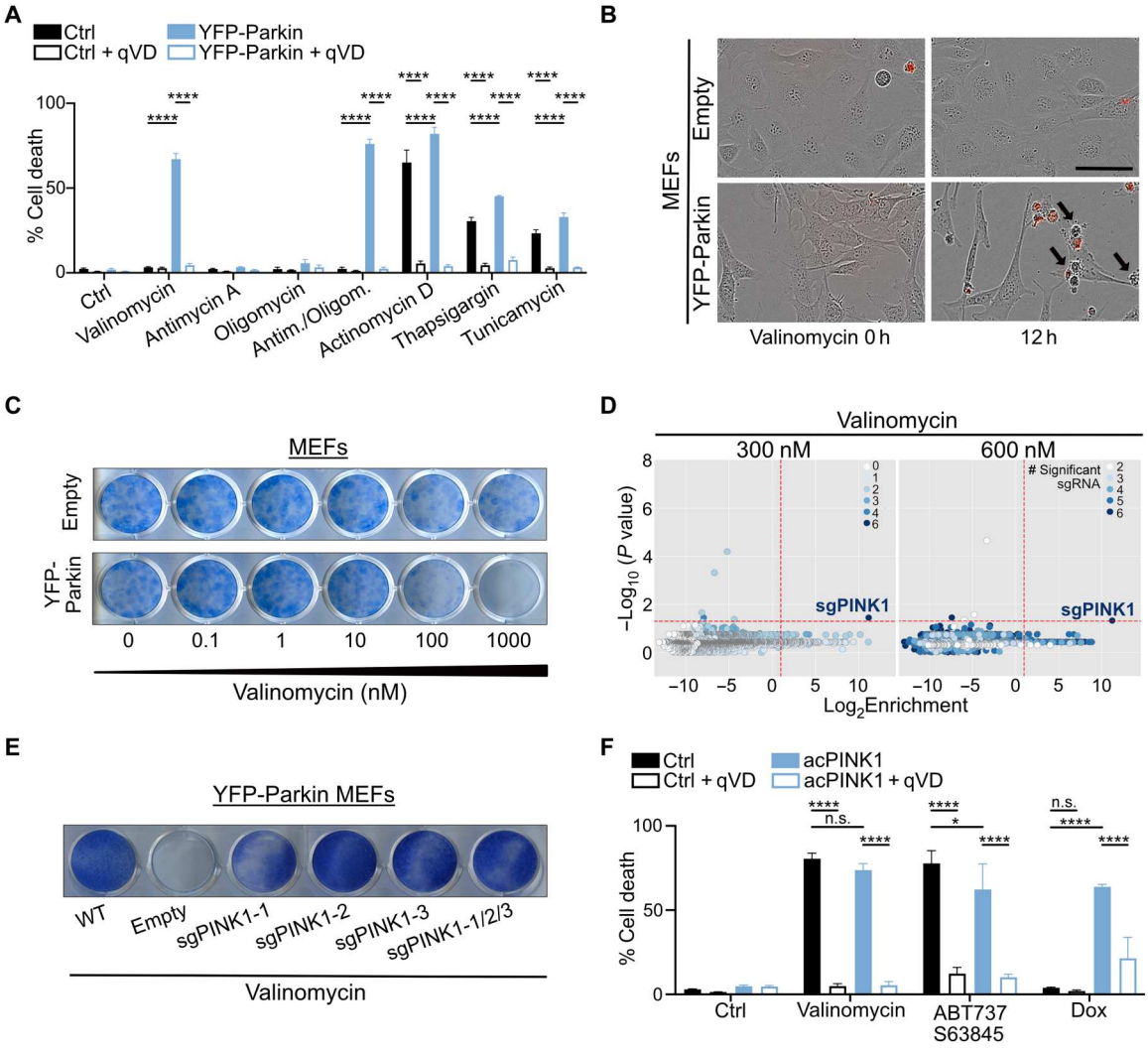

Fig. 1. Parkin expression sensitizes cells to apoptosis and requires PINK1. (**A**) Cell death quantification by IncuCyte of wild-type (WT) or YFP-Parkin MEFs after 24 hours of treatment with 5 μM valinomycin, additional mitochondrial toxins (5 μM antimycin A plus 1 μM oligomycin), or inducers of intrinsic apoptosis (1 μM actinomycin D, 1 μM thapsigargin, and 1 μM tunicamycin) in combination or not with 40 μM qVD. (**B**) Representative IncuCyte images showing PI positivity (red) and cell death morphology (black arrows) in WT or YFP-Parkin MEFs, related to (A). Scale bar, 70 μm. (**C**) Clonogenic assay of WT or YFP-Parkin MEFs after 2 hours of treatment with 600 nM valinomycin. (**D**) Results of CRISPR screen indicating single guide RNA (sgRNA) enrichment. (**E**) Clonogenic assay of YFP-Parkin MEFs expressing individual or the combination of three sgRNA, targeting *Pink1* after 15 min of treatment with 600 nM valinomycin. (**F**) Cell death quantification by IncuCyte of YFP-Parkin HCT116 with a doxycycline (Dox)–inducible active form of PINK1 (acPINK1) after 24 hours of treatment with 2.5 μM valinomycin, BH3 mimetics (5 μM ABT737 plus 5 μM S63845), or Dox (1 μg/ml), with or without 40 μM qVD. Error bars in (A) and (F) represent the SD of the means of triplicate samples. Data are representative of $n = 4$ (A), (B), and (F) or $n = 3$ (C) and (E) independent experiments. *$P < 0.05$; ***$P < 0.001$; n.s., not significant.

BAK but in a manner that required cyt c release into the cytosol and subsequent APAF1 activation.

Last, because the induction of cell death by valinomycin has been previously associated with antitumor activity both in vitro and in vivo (*36*–*38*), we sought to determine whether the observed Parkin-mediated apoptosis, in the absence of BAX and BAK, could engage tumor control in vivo. To this end, we implanted *Bax*$^{-/-}$ *Bak*$^{-/-}$ MEFs expressing or not YFP-Parkin into the flanks of nonobese diabetic *scid gamma* (NSG) immunodeficient mice and monitored tumor growth and survival. Notably, only the Parkin-expressing tumors were sensitive to valinomycin treatment that led to reduced tumor volume and improved survival (Fig. 2, H and I), consistent with our in vitro observations.

A genome-wide small interference RNA screen identifies genes regulating Parkin-dependent apoptosis

To investigate the molecular events that lead to the activation of Parkin-dependent apoptosis, we conducted a genome-wide small interference RNA (siRNA) screen in valinomycin-treated *Bax*$^{-/-}$ *Bak*$^{-/-}$ YFP-Parkin MEFs and measured Casp3/7 activity coupled to a high-content optical imaging system (fig. S3A). We identified genes whose silencing either inhibited or increased Parkin-dependent caspase activation (named "Class 1" and "Class 2," respectively) (Fig. 3A; fig. S3, B and C; and table S2). Among the Class 1 members, we identified several genes known to regulate apoptosis, such as *Apaf1*, cyt c somatic (*Cycs*; encoding cyt c), Holocytochrome C Synthase (*Hccs*) (*39*), and *Casp3* (*31*, *40*), as well as

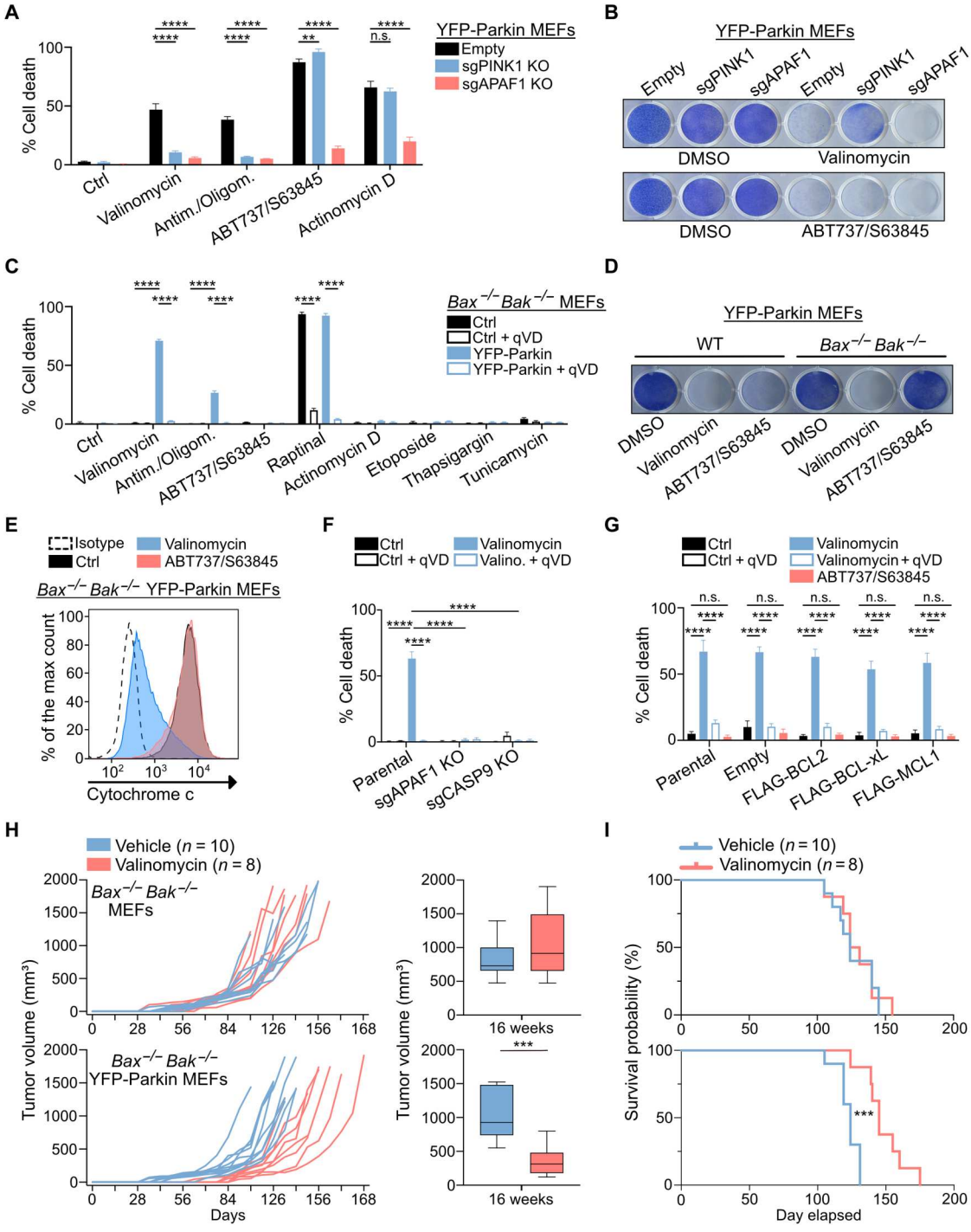

Fig. 2. Parkin-mediated apoptosis is BAX/BAK-independent. (**A**) Cell death quantification by IncuCyte of YFP-Parkin MEFs parental, sgRNA PINK1 KO (sgPINK1 KO), and sgAPAF1 KO after 24 hours of treatment with 5 μM valinomycin, 5 μM antimycin A plus 1 μM oligomycin (Antim./Oligom.), or inducers of intrinsic apoptosis (1 μM actinomycin D and 5 μM ABT737 plus 5 μM S63845). (**B**) Clonogenic survival assay of YFP-Parkin MEFs parental, sgPINK1 KO, and sgAPAF1 KO after 15 min of treatment with 600 nM valinomycin for 2 hours with BH3 mimetics (5 μM ABT737 plus 5 μM S63845). (**C**) Cell death quantification by IncuCyte of *Bax*$^{-/-}$ *Bak*$^{-/-}$ MEFs with or without YFP-Parkin after 24 hours of treatment as in (A) and (B) ± 40 μM qVD. (**D**) Clonogenic survival assay of WT or *Bax*$^{-/-}$ *Bak*$^{-/-}$ MEFs expressing YFP-Parkin, after 20 min of treatment as in (B). (**E**) MOMP quantification (see Materials and Methods) in *Bax*$^{-/-}$ *Bak*$^{-/-}$ YFP-Parkin MEFs after 6 hours of treatment as in (B). (**F**) Cell death quantification by IncuCyte of the indicated *Bax*$^{-/-}$ *Bak*$^{-/-}$ YFP-Parkin MEFs after 24 hours of treatment as in (A) and (B). (**G**) Cell death quantification by IncuCyte of *Bax*$^{-/-}$ *Bak*$^{-/-}$ YFP-Parkin MEFs expressing the indicated proteins after 24 hours of treatment with 2 μM valinomycin or BH3 mimetics (5 μM). (**H**) Flank tumor growth (left) and volume after 16 weeks (right) following the injection of nonobese diabetic *scid gamma* mice with *Bax*$^{-/-}$ *Bak*$^{-/-}$ MEFs with or without YFP-Parkin and treated peritumorally with vehicle or valinomycin (0.4 mg/kg) at days 4 and 8 after cells injection. (**I**) Survival curves of mice related to (H). Data in (A), (C), (F), and (G) represent means ± SD of triplicate samples. Data are representative of $n = 4$ (A) and (C), $n = 2$ (F) and (G), or $n = 3$ (B), (D), (H), and (I) independent experiments. DMSO, dimethyl sulfoxide. ***$P < 0.001$; ****$P < 0.0001$; n.s., not significant.

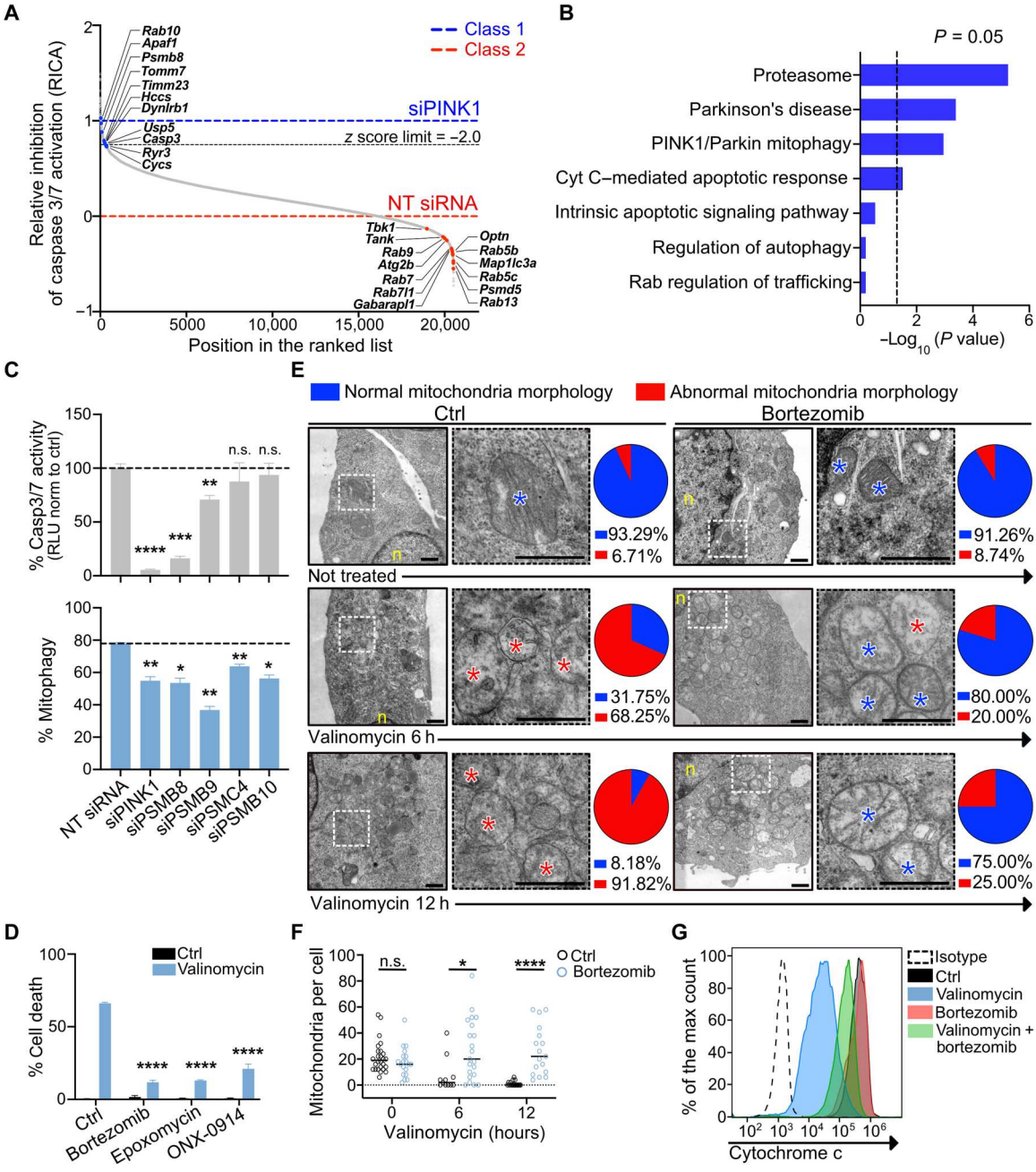

Fig. 3. Genes regulating Parkin-dependent apoptosis and the role of proteasomal activity in mediating OMM breaks and cyt c release in the cytosol. (**A**) Relative inhibition of Casp3/7 activation (RICA) in *Bax*$^{-/-}$ *Bak*$^{-/-}$ YFP-Parkin MEFs subjected to a genome-wide siRNA screen after 6 hours of treatment with 500 nM valinomycin (blue dashed line, RICA of siPINK1; red dashed line, RICA NT siRNA). Blue dots (Class 1) indicate genes that behave similarly to *Pink1* ($Z > -2.0$). Red dots (Class 2) indicate genes that increase Casp3/7 activity when compared to NT siRNA. (**B**) GSEA analysis showing significant enrichment of cellular processes containing candidate genes from Class 1. (**C**) Percentage of Casp3/7 activity in *Bax*$^{-/-}$ *Bak*$^{-/-}$ YFP-Parkin MEFs as relative light units (RLU) normalized to NT siRNA (top) and percentage of mitophagy by flow cytometry analysis (bottom) after 48 hours of siRNA silencing of the indicated proteins and 9 hours of treatment with 1 μM valinomycin. (**D**) Cell death quantification by IncuCyte of *Bax*$^{-/-}$ *Bak*$^{-/-}$ YFP-Parkin MEFs after 24 hours of treatment with 2.5 μM valinomycin plus 0.1 μM bortezomib, 0.1 μM epoxomicin, or 1 μM ONX-0914. (**E**) Transmission electron microscopy (TEM) analysis of *Bax*$^{-/-}$ *Bak*$^{-/-}$ YFP-Parkin MEFs after 6 and 12 hours of treatment with 2.5 μM valinomycin, 20 μM qVD, ± 0.1 μM bortezomib. Normal (blue) and abnormal (red) mitochondrial morphology are indicated by asterisks and reported per cell and as pie chart. n, nucleus. Scale bars, 0.98 μm. One representative image from each condition, $n \geq 11$. (**F**) Absolute numbers of normal mitochondria scored on per cell basis in TEM. Each condition, $n \geq 11$. (**G**) MOMP assessed by fluorescence-activated cell sorting (FACS) of *Bax*$^{-/-}$ *Bak*$^{-/-}$ YFP-Parkin MEFs treated with 1 μM valinomycin, qVD, ± 10 μM bortezomib. Means ± SD of triplicate samples (C) and (D). Data are representative of $n = 3$ (C), (D), and (G) independent experiments. *$P < 0.05$; **$P < 0.01$; ***$P < 0.001$; ****$P < 0.0001$; n.s., not significant.

genes previously characterized as regulators of PINK1 stability, such as *Tomm7* and translocase of inner mitochondrial membrane 23 (*Timm23*) (*7*). We also identified RAB10, member RAt Sarcoma virus (RAS) oncogene family (*Rab10*), a small guanosine triphosphatase (GTPase) that accumulates on mitochondria after depolarization and regulates mitophagy (*41*); ryanodine receptor 3 (*Ryr3*), which has been previously associated with the process of autophagic cell death (*42*); dynein light chain roadblock-type 1 (*Dynlrb1*), which is part of the cytoplasmic dynein complex and regulates traffic-induced degradation response for secretion (*43*, *44*); and ubiquitin specific peptidase 5 (*Usp5*), a member of the deubiquitinating enzymes (*45*). Class 2 members that increased caspase activation are discussed below.

To identify potential regulatory pathways of Parkin-mediated cell death, we subjected the identified candidate Class 1 genes to gene set enrichment analysis (GSEA) (Fig. 3B and fig. S3D). The most significant pathways included the following: "proteasome," "parkinson disease," "PINK1/Parkin-mediated mitophagy," and "cyt c-mediated apoptosis response." Notably, in accordance with the observation that Parkin-dependent cell death is independent of BAX and BAK function and regulation, GSEA did not identify pathways related to intrinsic apoptosis signaling, which is regulated by Bcl2 family members. Furthermore, pathways such as "regulation of autophagy" and "Rab regulation of trafficking" were not significantly enriched, suggesting that after valinomycin treatment, although YFP-Parkin MEFs undergo mitophagy (fig. S1E), genes required for the final stage of lysosomal degradation during autophagy might not be necessary for this Parkin-dependent process of apoptosis. Together, our genome-wide siRNA screen defined two major classes of genes that regulate the process of Parkin-dependent cell death in either a positive or negative manner.

Proteasomal activity mediates OMM breaks and cyt c release into the cytosol

We then focused on the "proteasome" gene signature, as it was the most significantly enriched pathway for Class 1 members. To validate this result, we selected the proteasome 26*S* subunit adenosine triphosphatase 4 (*Psmc4*) as representative of the canonical proteasome as well as the proteasome 20*S* subunit beta 8 (*Psmb8*), *Psmb9*, and *Psmb10* as components for the immune proteasome (fig. S3, D to F). siRNA silencing of these genes protected the $Bax^{-/-}$ $Bak^{-/-}$ YFP-Parkin MEFs from apoptosis induced by valinomycin, and consistent with previous reports (*46*), silencing of these genes also delayed mitophagy (Fig. 3C and fig. S3G). Moreover, either inhibitors of the proteasome, such as bortezomib and epoxomicin, or the inhibitor of the immune proteasome ONX-0914 protected $Bax^{-/-}$ $Bak^{-/-}$ YFP-Parkin MEFs from valinomycin-induced apoptosis (Fig. 3D), as well as from mitophagy (fig. S3H) (*10*–*13*).

Because one of the known functions of the proteasome is to degrade ubiquitinated proteins on the OMM (*13*), we hypothesized that this activity could create breaks in the OMM, leading to the observed release of cyt c into the cytosol upon valinomycin treatment. We therefore conducted an electron microscopy analysis on $Bax^{-/-}$ $Bak^{-/-}$ YFP-Parkin MEFs treated at different time points with valinomycin in combination or not with bortezomib and assessed mitochondrial integrity (Fig. 3E). When compared to control samples, cells treated with valinomycin showed mitochondria with abnormal morphology, typified by an enlarged shape and a reduced number of cristae, and breaks in or a total lack of OMM. This pattern became more evident at the latest time point, where the presence of normal mitochondria on a per cell basis decreased by 80% in the valinomycin-treated samples. Consistent with previous observations (*13*), the presence of bortezomib largely rescued the mitochondrial morphology even after 12 hours of cotreatment with valinomycin, as well as preserved the total number of normal mitochondria per cell (Fig. 3, E and F).

We then asked whether the rescued mitochondrial integrity would consequently lead to a decreased release of cyt c from the mitochondria upon proteasome inhibition. Bortezomib treatment reduced the amount of cyt c released to the cytosol during valinomycin-induced MOMP (Fig. 3G). These results, together with our previous observations, pointed to a mechanism in which Parkin-mediated ubiquitination triggers proteasome-dependent degradation of the OMM, consequent release of cyt c into the cytosol, activation of caspases, and ultimately apoptosis (fig. S3I).

A phenotypic classification model identifies genes mediating apoptosis

Next, we designed a secondary follow-up siRNA screen with the intention of validating the 313 candidate hits from the Class 1 members that showed a high relative inhibition of Casp3/7 activation (RICA). First, we narrowed the list of hits by excluding genes known to be indispensable for cell viability or siRNAs that induced either cytotoxicity or impaired expression of YFP-Parkin (fig. S4A). Then, we used this list of siRNAs to perform a siRNA screen in valinomycin-treated $Bax^{-/-}$ $Bak^{-/-}$ YFP-Parkin MEFs and assessed Casp3/7 activity. We identified a validated population of 170 genes with a RICA value higher than 0.5, recapitulating the phenotype of protection from caspase activation after treatment with valinomycin (table S3).

Following mitochondrial damage, Parkin translocates to the impaired mitochondria (*2*), and this event precedes cell death. We therefore reasoned that our observed process of cell death might be controlled at two different stages. To investigate this, we asked whether our validated list of hits could include genes that regulate the initial process of Parkin translocation to mitochondria and, therefore, caspase activation ("Class 1a"), in addition to genes that regulate only the later process of apoptosis but not Parkin translocation ("Class 1b") (fig. S4B).

For this purpose, we took advantage of the intracellular fluorescence signal of YFP-Parkin being cytosolic and diffuse in physiological conditions but clustered and unevenly distributed after treatment with mitochondrial uncouplers. While $Bax^{-/-}$ $Bak^{-/-}$ YFP-Parkin MEFs treated with a non-targeting siRNA (NT siRNA) showed a clustered, perinuclear YFP-Parkin localization (Fig. 4A, left), PINK1 siRNA inhibited Parkin translocation, resulting in a homogenous distribution of YFP-Parkin fluorescence in the cytosol, even if cells were treated with valinomycin (Fig. 4A, right).

We then developed a machine learning algorithm, based on YFP-Parkin clustering after valinomycin treatment (fig. S4, C to E), which defined type "A" and "B" cellular subtypes with reduced or increased translocation of YFP-Parkin onto the mitochondria, respectively (Fig. 4A, bottom). We then calculated a relative inhibition of YFP-Parkin translocation (RIPT) value that we used to differentiate Class 1a from Class 1b genes (Fig. 4B and table S3).

Tomm7, which is important for PINK1 stabilization and Parkin translocation (*7*), was identified as a member of Class 1a genes, showing a high RIPT value (fig. S4C). In contrast, classic apoptotic

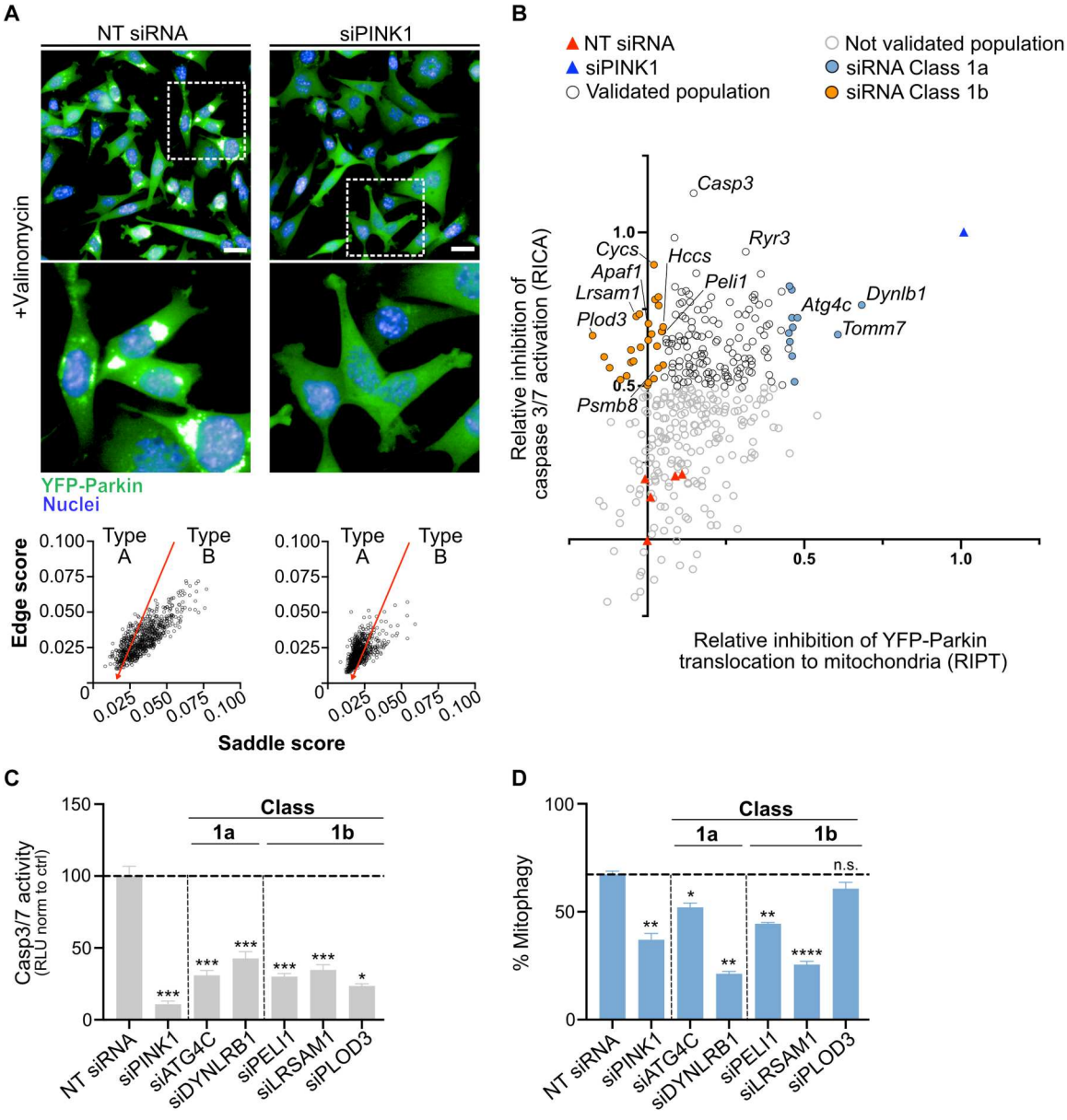

Fig. 4. A phenotypic classification model identifies genes mediating apoptosis. (**A**) Representative microscopy images showing YFP-Parkin localization and corresponding quantification of Edge and Saddle scores using a phenotypic classification model for per cell–based YFP-Parkin translocation. On the *XY* plot, the red line delineates the limit separating type A and B cells. After 48 hours of siRNA silencing, $Bax^{-/-}$ $Bak^{-/-}$ YFP-Parkin MEFs were treated with 500 nM valinomycin for 5 hours. Top, ×60 magnification; the bottom shows digital magnification of the corresponding white dotted square. Scale bars, 20 μm. (**B**) Bidimensional distribution of a subset of genes subjected to a secondary validation siRNA screen; data are plotted as RICA (*Y* axis) and relative inhibition of YFP-Parkin translocation to mitochondria (RIPT) (*X* axis). Samples treated with siPINK1 and valinomycin were centered at *X*,*Y* = 1,1; samples treated with NT siRNA and valinomycin were centered at *X*,*Y* = 0,0. (**C**) Percentage of Casp3/7 activity, as RLU normalized to NT siRNA, of $Bax^{-/-}$ $Bak^{-/-}$ YFP-Parkin MEFs after silencing of the indicated genes and 9 hours of treatment with 1 μM valinomycin. (**D**) Flow cytometry analysis showing percentage of mitophagy, quantified as lysosomal-positive mt-mKeima, after silencing of the indicated genes and 9 hours of treatment with 1 μM valinomycin. Error bars in (C) and (D) represent the SD of the means of triplicate samples. Data are representative of $n = 3$ independent experiments. *$P < 0.05$; **$P < 0.01$; ***$P < 0.001$; ****$P < 0.0001$; n.s., not significant.

genes such as *Apaf1*, *CytC*, *Hccs*, and *Casp3* as well as the proteasome subunit *Psmb8* were characterized as Class 1b members, supporting the notion that none of those genes regulate the initial step of Parkin translocation onto mitochondria.

To further test our classification, we used individual siRNAs to validate the Autophagy Related 4C Cysteine Peptidase (*Atg4c*) and the *Dynlrb1* as members of the Class 1a and the Pellino E3 Ubiquitin Protein Ligase 1 (*Peli1*), Leucine Rich Repeat and Sterile Alpha Motif Containing 1 (*Lrsam1*), and Procollagen-Lysine,2-Oxoglutarate 5-Dioxygenase 3 (*Plod3*) as members of the Class 1b. As predicted, the silencing of each of the tested genes was protected from caspase activation following valinomycin treatment, supporting the

validity of our phenotypic classification model algorithm (Fig. 4C and fig. S4F). In addition, the validated genes in Class 1a, restraining Parkin translocation, not only inhibited caspase activation but also mitophagy (Fig. 4D). This was not the case for all the validated members belonging to Class 1b. Among them, *Peli1* and *Lrsam1*, which are both E3 ubiquitin protein ligases capable of mediating proteasomal degradation and autophagy (*47*, *48*), also inhibited Parkin-dependent mitophagy. However, *Plod3* specifically inhibited apoptosis but failed to influence the process of autophagy-dependent mitochondrial degradation. Therefore, using our phenotypic classification model algorithm, we generated a useful framework for better understanding and characterizing the different steps of the observed Parkin-dependent apoptosis.

Failure in autophagy accelerates Parkin-dependent apoptosis

We next focused our attention on the Class 2 genes, as identified by our genome-wide siRNA screen, whose silencing exacerbated caspase activation when compared to NT siRNA samples (Fig. 3A). Pathway enrichment analysis on this set of genes showed significant enrichment for pathways such as "lysosome," "phagosome," "vesicle organization," "regulation of macroautophagy," "vesicular acidification," and "autophagosome organization" (Fig. 5A).

Considering these results, we hypothesized that the activity of the autophagy machinery and lysosomal degradation are crucial for segregating and degrading mitochondria that otherwise promote apoptosis. To test this, we first interrogated some of the hits that belonged to the Rab family of small GTPases, such as *Rab5* and *Rab7*, which play a central role in controlling autophagosome and lysosomal trafficking (*49*) and regulating mitophagy (*50*), and *Rab9*, which has been shown to mediate an alternative degradative pathway, driving small portions of mitochondria directly to lysosomal degradation (fig. S5A) (*51*).

In line with our screening results, we validated that $Bax^{-/-}$ $Bak^{-/-}$ YFP-Parkin MEFs treated with valinomycin and lacking *Rab7*, as well as the three isoforms of *Rab5* or *Rab9*, showed reduced mitophagy when compared to an NT siRNA sample (Fig. 5B, bottom). This delay in mitophagy was accompanied by a marked increase in caspase activation (Fig. 5B, top), suggesting that the inhibition of lysosomal maturation leads to a pronounced acceleration of cell death. Similarly, $Atg3^{-/-}$ YFP-Parkin MEFs, which lack ATG8 lipidation, were mitophagy deficient when treated with valinomycin or the combination of antimycin A and oligomycin (fig. S5, B and C) but were fully capable of undergoing apoptosis (Fig. 5C).

Parkin-dependent ubiquitination of OMM proteins leads to UPS- (*3*) or autophagy-mediated degradation (fig. S5D) (*52*). We observed that, although these two processes were both triggered by Parkin activity and mediated mitochondrial degradation, they exhibited opposite effects on cell death (Fig. 3 and Fig. 5, B and C). The discriminating factor between these two pathways is the recruitment of the ubiquitin binding autophagy receptors, five of which were previously characterized in the context of mitophagy (*14*). Among them, optineurin (*Optn*) was identified as a Class 2 member (Fig. 3A). We therefore postulated that the specific recognition of OMM-ubiquitinated proteins by autophagy receptors is a fate decision point in the context of Parkin-dependent apoptosis.

To test this hypothesis, we used HeLa ATG-R 5KO cells, which lack the five autophagy receptors: Tax1 Binding Protein 1 (TAX1BP1), calcium binding and coiled-coil domain 2 (NDP52), NBR1 autophagy cargo receptor (NBR1), sequestosome 1 (SQSTM1), and OPTN (*14*). These YFP-Parkin HeLa ATG-R 5KO cells showed a strong increase in caspase activation upon valinomycin treatment when compared to their wild-type (WT) counterpart (Fig. 5D) but were defective in mitophagy (fig. S5, E and F).

After cargo recognition through their ubiquitin binding domain, the autophagy receptors bind to ATG8 family members using their respective LIR domain (*53*). HeLa cells express six members of the highly conserved Atg8 family: LC3A, LC3B, LC3C, γ-aminobutyric acid Type A Receptor-Associated Protein (GABARAP), GABARAP-like 1 (GABARAPL1), and GABARAPL2. Two of them, *Gabarapl1* and *Lc3a*, were identified as Class 2 genes (Fig. 3A). Therefore, we evaluated the effect of valinomycin treatment in YFP-Parkin HeLa cells deficient for the LC3 (LC3 TKO), GABARAP (GABARAP TKO), or all members of the ATG8 family (6KO) (*54*). Consistent with the results observed in cells lacking the autophagy receptors, we observed enhanced caspase activity (compared to the WT line) after valinomycin treatment in the two TKO cell lines, which appeared additive in the 6KO line (Fig. 5D).

Following mitochondrial damage, TANK Binding Kinase 1 (TBK1) mediates recruitment of the autophagy receptors OPTN, NDP52, and SQSTM1 to depolarized mitochondria (*55*). Both *Tbk1* and its binding partner TRAF (tumor necrosis factor receptor–associated factor) family member–associated NF-κB (nuclear factor κB) activator (*Tank*) were also found among our Class 2 members. We therefore addressed their role in our model system, and, in line with the previously analyzed Class 2 members, $Bax^{-/-}$ $Bak^{-/-}$ YFP-Parkin MEFs treated with the TBK1 inhibitor BX-795 showed a substantial reduction in valinomycin-induced mitophagy (*56*) and increased caspase activation and apoptosis (Fig. 5E and fig. S5, G to I).

To test whether TBK1 regulates cell death through its action on autophagy receptors, we treated HeLa ATG-R 5KO with valinomycin in combination with BX-795. While BX-795 treatment increased caspase activation in YFP-Parkin HeLa WT cells, it did not have any effect on YFP-Parkin HeLa ATG-R 5KO cells, supporting a model in which TBK1 negatively regulates Parkin-dependent cell death by facilitating the recruitment of autophagy receptors to damaged mitochondria (Fig. 5E).

Previous studies have shown that the engagement of the mitochondrial pathway of apoptosis can induce the integrated stress response, as evidenced by eukaryotic translation initiation factor 2A (eIF2α) phosphorylation and expression of activating transcription factor 4 (ATF4) (*57*). Similarly, such engagement can induce type I interferon (IFN) responses when caspases are inhibited, because of the activation of the cyclic guanosine monophosphate-adenosine monophosphate synthase (cGAS)-stimulator of interferon genes (STING) pathway by released mitochondrial DNA (*58*, *59*). Consistent with these findings, we observed that treatment of Parkin-expressing HeLa cells with valinomycin in the presence of the caspase inhibitor, qVD, robustly induced eIF2α phosphorylation and ATF4 expression (Fig. 5F) as well as expression of several IFN response genes (Fig. 5G). It remains unclear how mitophagy may regulate these processes.

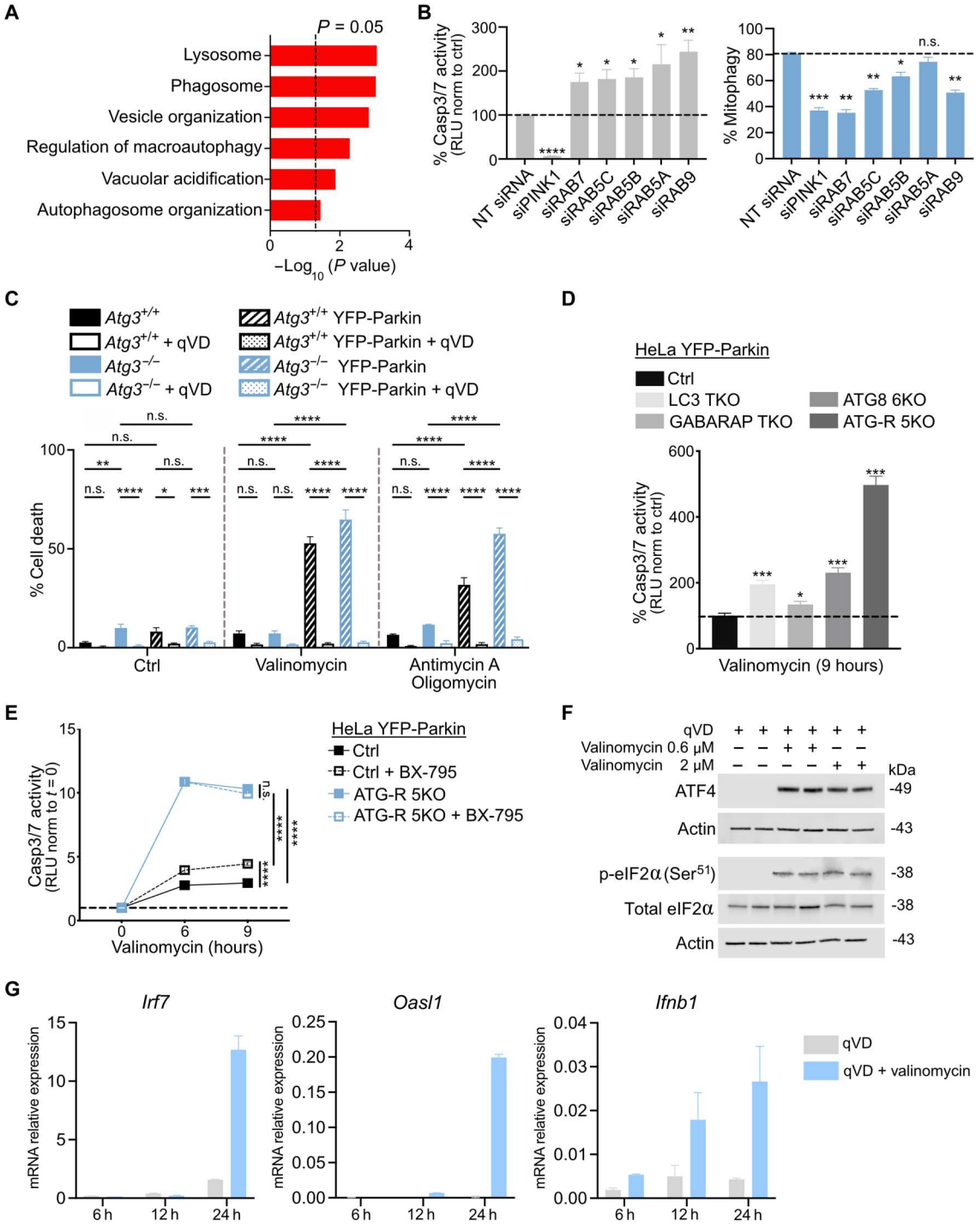

Fig. 5. Failure in autophagy accelerates Parkin-dependent apoptosis. (**A**) Overrepresentation enrichment analysis showing significant enrichment of pathways containing candidate genes from the Class 2 members with a RICA < 0 as related to Fig. 3A. (**B**) (Top) Percentage of Casp3/7 activity as RLU normalized to NT siRNA; (bottom) percentage of mitophagy by flow cytometry analysis after 48 hours of siRNA silencing of the indicated Rab family members and 9 hours of treatment with 1 μM valinomycin. (**C**) Cell death quantification by IncuCyte of $Atg3^{+/+}$ and $Atg3^{-/-}$ YFP-Parkin MEFs after 24 hours of treatment with 2.5 μM valinomycin or 5 μM antimycin A plus 1 μM oligomycin. (**D**) Percentage of Casp3/7 activity as RLU normalized to control in HeLa cells WT, LC3 TKO, GABARAP TKO, ATG8 6KO, and ATG-R 5KO, all expressing YFP-Parkin, after 9 hours of treatment with 1 μM valinomycin. (**E**) Casp3/7 activity normalized to time (*t*) = 0 in HeLa YFP-Parkin WT and YFP-Parkin ATG-R 5KO after 6 and 9 hours of treatment with 1 μM valinomycin in combination or not with 1 μM BX-795. (**F**) Immunoblot analysis showing expression of ATF4, total eIF2α, and phospho-eIF2α in $Bax^{-/-}$ $Bak^{-/-}$ YFP-Parkin MEFs treated for 24 hours with 40 μM qVD or qVD plus the indicated doses of valinomycin. (**G**) Quantitative polymerase chain reaction–relative mRNA expression of *Irf7*, *Oasl1*, and *Ifnb1* genes in $Bax^{-/-}$ $Bak^{-/-}$ YFP-Parkin MEFs treated with 40 μM qVD or qVD plus 2 μM valinomycin for the indicated hours. Error bars in (B), (C), (E), and (G) represent the SD of the means of triplicate samples. Data are representative of (B), (C), and (E) *n* = 3 or (G) *n* = 2 independent experiments. Error bars in (D) represent the SD of the mean of *n* = 3 independent experiments.

In conclusion, our results suggest that ubiquitinated OMM proteins can be degraded by UPS, thereby increasing OMM rupture, cyt c release, and cell death. Alternatively, they can be recognized by autophagy receptors, triggering the engulfment of mitochondria into autophagosomes and driving autophagic degradation of damaged mitochondria. These contrasting effects dictate cell fate in Parkin-expressing cells in response to mitochondrial depolarization.

DISCUSSION

We found that Parkin expression sensitizes cells to die after treatments that depolarize mitochondria. PINK1 was necessary and sufficient to drive this Parkin-dependent cell death. It is therefore conceivable that, in tissues or cell types expressing sufficiently high levels of Parkin, this form of cell death might take place physiologically in response to mitochondrial stressors.

Parkin-dependent cell death is associated with caspase activation and therefore is a bona fide apoptosis that requires APAF1 activation and cyt c release from the intermembrane space (*26*). In the absence of caspase activity, cells nevertheless died, likely because of catastrophic mitochondrial damage, similar to that of caspase-independent cell death following MOMP (*32*). Our genetic approach showed that Parkin-dependent cell death did not require the effectors BAX and BAK. Previous reports have suggested a central role for MCL1 in a similar BAX- and BAK-independent cell death (*23*, *24*); however, in our experimental setting, neither BCL2, BCL-xL, nor MCL1 regulated cyt c release and the subsequent extent of apoptosis. Thus, Parkin-mediated apoptosis appears to overlap with known mechanisms of classical apoptosis downstream of cyt c release but remains mechanistically distinct at the level of outer membrane permeabilization.

Our observations are consistent with the literature describing the role of Parkin activity at the OMM in triggering mitophagy. During mitophagy, the UPS-mediated degradation of OMM proteins is followed by the complete degradation of mitochondrial remnants through autophagy. Using pharmacological or genetic approaches, coupled to the mitochondrial targeted probe for lysosomal degradation, mt-mKeima, we observed that the inhibition of either UPS or autophagy block lysosomal degradation of mitochondrial proteins. However, while inhibition of the UPS inhibited cell death, inhibition of autophagy did not, suggesting that the processes of mitochondrial degradation and cell death are differentially regulated downstream of the activation of the UPS. Therefore, our observations on Parkin-dependent cell death cannot be explained in light of the previously described process of autophagic cell death (*29*).

While our genome-wide CRISPR screen identified *Pink1* as the only gene regulating cell death upstream of Parkin, our siRNA screen and the following validation with a machine learning algorithm for the analysis of Parkin translocation onto mitochondria gave us a more nuanced picture defined by a complex set of genes involved in the regulation of this form of cell death. With this approach, we identified major intracellular pathways that positively or negatively regulate this process. While, the UPS was confirmed as necessary for the induction of cell death, the inhibition of pathways regulating autophagy and lysosomal function accelerated cell death. Among them, and in line with a previous report (*60*), we found that several members of the Rab small GTPase family, which play a major role in the autophagosome-lysosomal maturation process during mitophagy (*41*, *50*, *51*), increased caspase activation.

Our work also defines autophagy receptors as important in the cell fate decision between survival and cell death. Previous studies in *Drosophila* suggested that the ubiquitination status of the Voltage Dependent Anion Channel 1 (VDAC1) is an important discriminant between mitophagy and cell death in the context of Parkin activation (*25*). Considering our results, it is conceivable that the VDAC1 ubiquitination status determines its ability to recruit autophagy receptors. Moreover, our model could explain, at least in part, previous observations involving autophagy receptors. For instance, mutations in *Optn*, which reduced OPTN levels and/or activity, were associated with neurodegeneration and cell death (*61*) and have been reported to induce apoptosis, which was antagonized by autophagy (*62*). Furthermore, the activity of the autophagy receptors OPTN, NDP52, and SQSTM1 is regulated by TBK1-mediated phosphorylation (*55*), and similarly, RAB7A is regulated by TBK1 during mitophagy (*63*).

In our study, we observed that in the context of Parkin activation, pharmacological regulation of TBK1 had a major effect on the ability of cells to undergo programmed cell death. TBK1 therefore might represent a target for the development of future therapies in the context of cancer and neurodegenerative diseases.

MATERIALS AND METHODS

Cell lines

HeLa [American Type Culture Collection (ATCC), CCL-2], 293T (ATCC, CRL-3216), Phoenix-AMPHO (ATCC, CRL-3213), and primary MEFs were maintained at 37°C/5% (v/v) CO_2 in a humidified incubator in Dulbecco's modified Eagle's medium (Gibco, 11971–025) supplemented with 10% fetal bovine serum, 2 mM L-glutamine (Gibco, 25030-081), penicillin-streptomycin (100 U/ml; Gibco, 15140-122), 1 mM sodium pyruvate (Gibco, 11360-070), nonessential amino acids (Gibco, 11140-050), and 55 μM β-mercaptoethanol (Gibco, 21985-023). HCT116 (ATCC, CCL-247) were maintained in McCoy's 5 A medium (ATCC, 30-2207) and supplemented as above. MEFs were immortalized with the SV40 large T antigen (pBabe-Neo-SV40-LTA). WT HCT116, *Bax*$^{-/-}$ *Bak*$^{-/-}$ HCT116, and *Bax*$^{-/-}$ *Bak*$^{-/-}$ MEFs cell lines were a gift from R. Youle (*64*). For the generation of *Atg3*$^{-/-}$ YFP-Parkin MEFs, *Atg3*$^{f/f}$ mice (provided by H. W. Virgin) were bred to CMV-Cre mice (the Jackson Laboratory, 006054) for deletion of loxP-flanked genes in all tissues. The obtained *Atg3* heterozygous mice were subsequently mated to finally generate *Atg3*$^{-/-}$ KO MEFs. The following HeLa cells were provided by M. Lazarou: WT, LC3 TKO (lacking LC3A, LC3B, and LC3C), GABARAP TKO (lacking GABARAP, GABARAPL1, and GABARAPL2), ATG8 6KO (lacking the six ATG8 members), and ATG-R 5KO (lacking the five autophagy receptors TAX1BP1, NDP52, NBR1, SQSTM1, and OPTN) (*14*, *54*). Cell lines were routinely tested for mycoplasma using the MycoAlert Plus mycoplasma detection kit (Lonza).

Plasmids and retroviral transduction

For generating YFP-Parkin cells, the pLZRS-YFP-Parkin construct was cloned as previously described (*65*). To create the acPINK1-inducible system, OPA3-PINK1 Δ1–110, provided by R. Youle (*6*), was subcloned into the Dox-inducible vector pRetroX-TRE3G

(Clontech, 631188) as previously described (*66*). To stably express the pH-sensitive mitochondrial mt-mKeima probe, cells were retrovirally transduced using the pCHAC-mt-mKeima plasmid, a gift from R. Youle (Addgene, 72342). All BCL2 family member cDNAs used in this study were of human origin; FLAG-BCL2, FLAG-BCL-xL, and FLAG-MCL1 were subcloned into the retroviral vector pMX-IRES-Cerulean as previously described (*66*). All stable cell lines were generated by retroviral transduction. Briefly, Phoenix-AMPHO (amphotropic) cells (0.5×10^6 per 10-cm dish) were transfected with retroviral constructs using Lipofectamine 2000 (Life Technologies, 11668027). Two days later, the virus-containing supernatant was harvested, filtered, and used to infect 1×10^5 target cells in the presence of hexadimethrine bromide (polybrene) (5 μg/ml; Sigma-Aldrich, H9268). Forty-eight hours postinfection, stable transductants were selected after adding puromycin (2 to 0.5 μg/ml; Sigma-Aldrich, P8833) or were sorted by flow cytometry for YFP positivity.

Reagents, cell death induction, and chemical inhibitors

The following reagents and concentrations were used, unless indicated otherwise: 0.3 to 5 μM valinomycin (Sigma-Aldrich, V0627), 5 μM antimycin A (Sigma-Aldrich, A8674), 1 μM oligomycin (Sigma-Aldrich, O4876), 1 μM actinomycin D (Sigma-Aldrich, A1410), 1 to 2 μM thapsigargin (ENZO, BML-PE180-0001), 1 to 2 μM tunicamycin [MedChemExpress (MCE), HY-A0098], 20 to 40 μM qVD (MCE, HY-12305), 5 μM ABT-737 (MCE, HY-50907), 5 μM S63845 (MCE, HY-100741), 5 μM raptinal (MCE, HY-121320), 100 μM etoposide (MCE, HY-13629), 1 μM rotenone (MCE, HY-B1756), 0.1 to 10 μM bortezomib (Cayman, 10008822), 0.1 μM epoxomycin (MCE, HY-13821), 1 μM ONX-0914 (Cayman, 16271), Dox (1 μg/ml; Clontech, 631311), and 1 μM BX-795 (MCE, HY-10514).

Mitochondrial potential measurement

Mitochondrial transmembrane potential was assessed using the potentiometric dye TMRE (Thermo Fisher Scientific, T669). A total of 50 nM TMRE dye was added to the cells for 5 min, and fluorescence was acquired by flow cytometry before (time 0) or after addition of 5 μM valinomycin or 5 μM antimycin A plus 1 μM oligomycin for the indicated time. The fluorescence emission of the dye was acquired with a 5-lasers Aurora (Cytek) spectral flow cytometer, and median fluorescence intensity (MFI) was analyzed using FlowJo (v10; Tree Star).

Mitochondrial reactive oxygen species measurement

Mitochondrial reactive oxygen species production was assessed using the Mitochondrial Superoxide Indicator MitoSOX-RED (Thermo Fisher Scientific, M36008). Cells were treated for the indicated times with 40 μM qVD or qVD plus 5 μM valinomycin. At the end of the treatment, cells were harvested using trypsin-EDTA (Corning, 25053CI) and washed, and 5 μM MitoSOX-RED was added to the collected cells for 30 min at 37°C and 5% CO_2. Cells were washed and the fluorescence emission of the dye was measured with a 5-lasers Aurora (Cytek) spectral flow cytometer, and MFI was analyzed using FlowJo (v10, Tree Star).

Cell death measurement

After the indicated treatment, cell death was quantified using a two-color IncuCyte Zoom in-incubator Imaging System (Sartorius). The percentage of cell death was obtained by normalizing the dead cell count with the total cell count detected by the uptake of 1 μg/ml of the cell-impermeable dye propidium iodine (PI) (Sigma-Aldrich, P4170) and 100 nM of the cell-permeant dye SYTO 16 (Invitrogen, S7578), respectively. Casp3/7 activity was assessed by luminescence using the Caspase-Glo 3/7 Assay System following manufacturing instructions (Promega, G8091).

Clonogenic assay

Cells were seeded in 24-well plates (5×10^4 per well) 24 hours before the assay. After treatment, wells were washed three times with phosphate-buffered saline (PBS), and fresh complete medium was added. After 5 to 7 days in culture, the plates were gently washed with PBS and then stained with methylene blue solution [1% (w/v) methylene blue in a 50:50 methanol/water solution] for 30 min at room temperature. The plates were then washes with distilled H_2O, air dried, and scanned using a document scanner.

Assessment of mitophagy by mt-mKeima flow cytometry assay

Mitophagy was assessed by flow cytometry with the mt-mKeima fluorophore that has bimodal excitation under neutral (440 nm) and acidic conditions (586 nm). Cells were seeded in 24-well plates (5×10^4 per well). The next day, cells were treated with compounds as specified in the figures, in the presence of 20 μM qVD. After treatment, cells were harvested with trypsin-EDTA (Corning, 25053CI), washed, and resuspended in annexin binding buffer (Invitrogen, V13246) in the presence of annexin-V–allophycocyanin (APC) (Biolegend, 640941) to exclude death cells. Mitophagy was quantified by detecting lysosomal mt-mKeima using dual-excitation ratiometric pH measurements at 488- or 405-nm (pH 7) and 561-nm (pH 4) lasers, as previously described (*14*, *46*). Data were analyzed using FlowJo (v10; Tree Star).

CRISPR-Cas9 genome editing of cell lines

Highly edited KO MEFs cells were generated using CRISPR-Cas9 technology using CRISPR All-in-One (pLenti-U6-sgRNA-SFFV-Cas9-2A-Puro) lentiviral vectors (ABMgood, C442). A set of three oligonucleotide pairs of sgRNAs per each gene was used: sgPINK1-1 (GCTGATCGAGGAGAAGCAGG), sgPINK1-2 (GATCTCCTGACAGGCCGAGG), sgPINK1-3 (TGCCAGCATCGAGTGTCCAG), sgAPAF1-1 (TGGCGTCTTGTCAGTGATG), sqAPAF1-2 (GGCTGCTCGTTGATATGAG), sgAPAF1-3 (TACAACGCTCTGCTACACGA), sgCASP9-1 (CTTCACGCGCGACATGATCG), sgCASP9-2 (TGTTAAACCCCTAGACCACC), and sgCASP9-3 (GGGGTGAGGTTTCCCACGGC). Single KO clones were generated by selecting the KO pools with puromycin (0.5 μg/ml) and sorting them for single cells by flow cytometry (St. Jude Flow Cytometry and Cell Sorting Immunology Facility). Deletions were confirmed by Western blot or by targeted next-generation sequencing (NGS).

CRISPR KO screen

The mouse CRISPR-Cas9 KO (GeCKOv2) pooled library was a gift from F. Zhang (Addgene, 1000000052), and it was used following a previously described protocol (*67*). Briefly, the gRNA pooled library in the vector lentiCRISPRv2 was amplified in Endura competent cells, and NGS was performed to determine sgRNA distribution. Lentivirus was then generated in human embryonic kidney 293T

cells and virus titer was determined. Target YFP-Parkin MEFs were lentivirally transduced with the library at 0.3 multiplicity of infection, treated or not with two concentrations of valinomycin (300 or 600 nM) for three rounds of treatment and enriched by clonogenic survival for pools of cells expressing multiple gRNAs targeting the same gene. Genomic DNA was harvested and prepared for NGS. For NGS analysis, reads were aligned using PinAPL-Py (http://pinapl-py.ucsd.edu/). Counts per million reads of samples treated with valinomycin were normalized to untreated samples, and two biological replicates were averaged to calculate the respective fold enrichment for each gRNA. The significance of each sgRNA was determined using one-sided permutation test. *P* value was calculated as the fraction of events when the enrichment was greater than 10,000 randomly chosen sgRNAs. Significance at the gene level was tested by performing a two-sided Welch's *t* test of the enrichment of the sgRNAs recovered for each gene against six randomly chosen sgRNAs. Data were displayed as negative logarithm of the gene-level *P* values against the mean enrichment and number of significant sgRNAs. Python scripts are available from the authors upon request. Validation of the candidate gene for the screening phenotype was performed by cloning three different sgRNAs into the plasmid backbone of the sgRNA library and by performing the screening workflow YFP-Parkin MEFs PINK1 KO single-cell clones, or the poll of the three different clones, as described above. NGS data have been deposited with links to BioProject accession number PRJNA956539 in the NCBI BioProject database (www.ncbi.nlm.nih.gov/bioproject/).

Cyt c release assay measured by flow cytometry

A total of 1×10^5 cells were seeded 1 day before the experiment. The next day, cells were treated with drugs in combination with 40 μM qVD to prevent caspase activation. After treatment, cells were harvested by trypsinization, washed twice with cold PBS, and permeabilized on ice with 500 μl of digitonin (25 μg/ml) in PBS for 10 min. After two washes with PBS/1 mM EDTA/1% bovine serum albumin [fluorescence-activated cell sorting (FACS) buffer], cells were resuspended in Fixation/Permeabilization buffer (BD, 554714) and incubated for 20 min on ice. Cells were then washed with BD Perm/Wash buffer and stained on ice in 50 μl of the same buffer with Alexa Fluor 647–conjugated anti–cyt c antibody (1:200; BioLegend, 612310) or mouse IgG1k Isotype Ctrl (Invitrogen, 51-4714-81) for 30 min. Last, cells were washed two more times with BD Perm/Wash buffer and resuspended in FACS buffer before flow cytometric analysis.

Assessment of tumor growth in vivo

A total of 1×10^6 $Bax^{-/-}$ $Bak^{-/-}$ MEFs expressing or not YFP-Parkin were resuspended in 100 μl of PBS and injected subcutaneously into the flanks of males NSG immunodeficient mice (the Jackson Laboratory, 005557). At days 4 and 8 after cell injection, mice were treated by peritumoral injection with vehicle or valinomycin (0.4 mg/kg). Tumor growth was measured every 7 days, and mouse survival was monitored. All mice were housed in pathogen-free facilities, in a 12-hour light/dark cycle in ventilated cages, with chow and water supply ad libitum. All animal procedures were performed in accordance with protocols approved by the Institutional Animal Care and Usage Committee of St. Jude Children's Research Hospital.

Genome-wide siRNA screen

Briefly, 20,518 mouse genes were screened using RNA interference (RNAi) for relief from PINK1/Parkin-dependent cell death (fig. S3A). $Bax^{-/-}$ $Bak^{-/-}$ YFP-Parkin MEFs were reverse-transfected using Dharmafect II (Dharmacon, T-2002-04) with 25 nM of a pool of four siRNAs (Mouse siGENOME siRNA Library, SMARTpool; Dharmacon, G-015005-E2-05), targeting each gene per well arrayed in a 384-well format. After 48 hours of RNAi knockdown, cells were challenged by addition of valinomycin (Sigma-Aldrich, V0627) to a final concentration of 500 nM. Six hours after valinomycin challenge, cell death activity was assayed using the Caspase-Glo 3/7 Assay System (Promega) and the luminescence for each well was quantified using the Envision Multilabel plate reader (PerkinElmer) (fig. S3A). For the primary screen, PINK1/Parkin-dependent cell death was evaluated relative to the negative control NT siRNAs (siGENOME NT siRNA #4; Dharmacon, D-001210-04) and the positive control PINK1 siRNA (siGENOME PINK1 siRNA SMARTpool; Dharmacon, M-044666-01). The luminescence for each well in the primary screen (table S2) was processed such that values were log transformed, adjusted for plate position bias using median polish, and two-point normalized where NT siRNA and PINK1 siRNA centered to the values 0 and 1, respectively, using Genedata Screener software. During the primary screen, a composite *Z'* factor of 0.42 was achieved, attesting to the robustness of the screening approach (table S2) (*68*, *69*). Candidate hits required for PINK1/Parkin-dependent cell death were selected after *z* score transformation using *Pink1* knockdown population mean and SD. A total of 313 gene knockdowns that compare favorably with *Pink1* knockdown (*z* score greater than −2.0) were selected and shown (fig. S3, B and C) as a RICA value close to 1. Those hits were defined as Class 1 and were identified as genes behaving as we observed for *Pink1*, where their silencing inhibited Parkin-dependent caspase activation. We also identified a second class (Class 2) of genes whose silencing increased caspase activation when compared to a NT siRNA treatment, therefore receiving, after normalization, negative RICA values.

Secondary follow-up screen

In total, 419 genes of interest (top hits and selected genes) were screened in a validation experiment. Fresh pools of four siRNAs were obtained from Dharmacon, and the RNAi knockdown was induced following a reverse transfection protocol similar to the primary screen. The 419 genes of interest were screened for relief from PINK1/Parkin-dependent cell death after valinomycin challenge following an experimental procedure similar to the primary screen (table S3). To extend the findings, RNAi-associated cell toxicity was directly interrogated 48 hours after siRNA transfection (in the absence of valinomycin challenge) using the CellTiter-Glo luminescent viability assay (Promega, G7572) and read using an Envision plate reader. In a separate experiment, YFP-Parkin expression was characterized after RNAi-induced gene knockdowns using automated imaging and image analysis. Hoechst staining and YFP-Parkin expression were captured using 405- and 488-nm laser excitations, respectively, of four fields per well using a GE InCell 6000 analyzer (GE Healthcare) at ×20 magnification. All data were then uploaded to the Columbus Image Data Storage and Analysis System (PerkinElmer) for image analysis. Nuclear and cytoplasmic boundaries were first segmented using staining from the 405 channel, and any objects not completely within the field of view were removed

from further analysis. Cells were additionally selected for analysis by passing minimum nuclear roundness and size thresholds. The mean YFP-Parkin intensity was measured for every cell, and the median value of that population was reported for each well. Thirty-five gene knockdowns negatively affected cell health (fig. S4A, left), and additional nine gene knockdowns were associated with reduced YFP-Parkin expression (fig. S4A, right). The validation screen identified 170 genes as required for PINK1/Parkin-dependent cell death.

Phenotypic classification model

A machine learning algorithm classified two cellular subtypes on the basis of the intracellular YFP-Parkin distribution after 5 hours of valinomycin treatment. Hoechst staining and Parkin-YFP expression were captured using 405- and 488-nm laser excitations, respectively, of nine fields per well using a GE InCell 6000 analyzer (GE Healthcare). All data were then uploaded to the Columbus Image Data Storage and Analysis System (PerkinElmer) (fig. S4, C and D) for image analysis. Nuclear and cytoplasmic boundaries were first segmented using staining from the 405 channel, and any objects not completely within the field of view were removed from further analysis. Cells were additionally selected for analysis by passing minimum nuclear roundness and size thresholds. The Columbus PhenoLOGIC algorithm (PerkinElmer) was then used to calculate the "Edge" and "Saddle" textures for each cell using a 2-pixel seed size. Last, once these textures were captured by the software, empirical classification was used in combination with machine learning to classify the cells into two subpopulations (fig. S4, D and E): type A cells, defined as events with a lower Saddle and Edge score and with a reduced translocation of YFP-Parkin onto the mitochondria after valinomycin treatment (YFP evenly distributed throughout the cells), and type B cells, with higher Saddle and Edge scores and with increased YFP-Parkin translocation onto the mitochondria (YFP accumulated in puncta). The number of cells in class "B" were then divided by the total cells in classes "A" and "B" to generate a single value per well to describe the fraction of cells with YFP-Parkin in distinct puncta. We then extrapolated a unique value describing YFP-Parkin translocation onto mitochondria (RIPT) and, after normalization, calculated a RIPT value that we used to differentiate Class 1a from Class 1b genes (Fig. 4B and table S3). As a negative and positive control, NT and PINK1 siRNAs were assigned a RIPT value of 0 and 1, respectively.

siRNA transient transfection

siRNA transient transfection was performed over 48 hours using Dharmafect II (Dharmacon, T-2002-04) with 25 nM of a mixture of a pool of four siRNAs (Dharmacon, Mouse siGENOME siRNA, SMARTpool), selected from the Mouse siGENOME siRNA Library, SMARTpool (Dharmacon, G-015005-E2-05). siRNA oligo sequences can be retrieved from the siRNA ID listed in table S2.

Pathway enrichment analysis

GSEA was performed against MSigDB database with R package clusterProfiler (version 3.18.1) (Fig. 3B and fig. S3D). RICA was used for gene ranking. Overrepresentation enrichment of the Class 2 members with a RICA < 0 was performed against MSigDB with R package clusterProfiler (version 3.18.1) (Fig. 5A). Moreover, to examine whether the enrichment was due to *Pink1* and *Prkn* (encoding for Parkin) in the gene sets, the two genes were excluded from the gene sets and similar results were obtained.

Electron microscopy

Samples for electron microscopy were fixed in 0.1 M cacodylate buffer containing 2.5% glutaraldehyde and 2% paraformaldehyde. Samples were postfixed in reduced osmium tetroxide and contrasted with aqueous uranyl acetate. Dehydration was by an ascending series of ethanol to 100% followed by 100% propylene oxide. Samples were infiltrated with EmBed-812 and polymerized at 60°C. Embedded samples were sectioned at ~70 nm on a Leica UC-7 ultramicrotome and examined in a Thermo Fisher Scientific TF20 transmission electron microscope at 80 kV. Digital micrographs were captured with an Advanced Microscopy Techniques imaging system controlled by SerialEM for acquiring montages of whole cells for analysis. Montages were stitched and exported as tiff files for analysis using the IMOD software (https://bio3d.colorado.edu/imod/). Unless otherwise indicated, all reagents were provided by Electron Microscopy Sciences.

Western blotting and antibodies

Cells were lysed in radioimmunoprecipitation assay buffer [50 mM tris-HCl (pH 7.4), 150 mM NaCl, 1% NP-40, 0.5% deoxycholic acid, and 0.1% SDS], complete protease inhibitors (Roche, 11836153001), or phosphatase inhibitors (Roche, 04906837001). Protein concentration was assessed by bicinchoninic acid (BCA) assay (Pierce, 23225) and normalized before Western blotting. Samples were run on 4–12% Criterion XT Bis-Tris Precast Gels (Bio-Rad) and transferred to Hybond-C Extra membranes (GE Healthcare). After antibody incubation and chemiluminescent substrate exposure (homemade ECL), membranes were acquired by a ChemiDoc Touch Imaging System (Bio-Rad) and analyzed by Image Lab software (Bio-Rad). The following antibodies were used for immunoblotting: anti-BAK (Santa Cruz Biotechnology, sc832), anti-BAX clone N-20 (Santa Cruz Biotechnology, sc493), anti-MCL1 (Rockland, 600–401–394), anti–β-actin clone C4 (Santa Cruz Biotechnology, sc47778), anti-Parkin (Santa Cruz Biotechnology, sc32282), anti–green fluorescent protein (Santa Cruz Biotechnology, sc8334), anti-PINK1 (Novus, BC100-494), anti-COX Vb (Abcam, ab110263), anti-PARP (Cell Signaling Technology, 9542), anti-APAF1 (Bio-Rad, AHP-487), anti-FLAG (Sigma-Aldrich, F7425), anti-Casp9 (Cell Signaling Technology, 9504), anti-ATG3 (Cell Signaling Technology, 3415), anti-ATF4 (Cell Signaling Technology, 11815), total eIF2α (Cell Signaling Technology, 9722), and phospho-eIF2α (Cell Signaling Technology, 9721).

Real-time quantitative polymerase chain reaction

Total RNA was extracted using the RNeasy Mini Kit (QIAGEN, 74104). Reverse transcription reaction was performed with M-MLV reverse transcriptase (Invitrogen, 28025013) and random hexamers (IDT). Real-time quantitative polymerase chain reaction (qPCR) was performed using SYBR Green (Invitrogen, 4309155) in a 7500 Fast Real-Time PCR System (Applied Biosystems) using the following PCR conditions: 50°C in 2 min, 95°C in 10 min, 45 cycles of 95°C in 15 s, and 60°C in 1 min. β-*actin* mRNA expression was used for normalization. The following primers (IDT) were used in this study: mouse_β-*actin* (forward: AGAGGGAAATCGTGCG TGAC; reverse: CAATAGTGATGACCTGGCCGT), mouse_*Pink1*

(forward: GGCTTCCGTCTGGAGGATTAT; reverse:AACCTGCC GAGATATTCCACA), mouse_*Psmb8* (forward: ATGGCGTTACT GGATCTGTGC; reverse: CGCGGAGAAACTGTAGTGTCC), mouse_*Psmb9* (forward: CATGAACCGAGATGGCTCTAGT; reverse: TCATCGTAGAATTTTGGCAGCTC), mouse_*Psmc4* (forward: CAGCACTGTCCGTGTCTCG; reverse: CTGCTCGTC CTTGATATACTCCT), mouse_*Psmb10* (forward: GAGGAATGC GTCCTTGGAACA; reverse: CAC AACCGAATCGTTAGTGGC), mouse_*Atg4c* (forward: AGATGAAAGCAAGATGTTGCCT; reverse: CCCTGTAGGTCAGCCATATTCTA), mouse_*Dynlrb1* (forward: AGCCAGAAAGGAGTGCAGG; reverse: GGGATTGT CCATTGTGCTCTTG), mouse_*Peli1* (forward: CAAGGACCAGC ATAGCATATCAT; reverse: GTTGACCGACCAATCTGAAACA), mouse_*Lrsam1* (forward: CTCGAAAACGCCTGGAGTACC; reverse: AGGTGAGGTGGTTTGTATGGA), mouse_*Plod3* (forward: AAGAAGTTTGTTCAGAGTGGCA; reverse: TGAATC CACCAGAGTTGAGGA), mouse_*Rab7* (forward: AAGCCACAA TAGGAGCGGAC; reverse: AGACTGGAACCGTTCTTGACC), mouse_*Rab5c* (forward: TGGTCCTCCGCTTTGTCAAG; reverse: TGACCGTTGTATCGTCTAAGCA), mouse_*Rab5b* (forward: GG GAAGTCTAGCCTGGTGTTA; reverse: GCTTTCCTGGTATT CATGGAACT), mouse_*Rab5a* (forward: GCTAATCGAGGA GCAACAAGAC; reverse: CCAGGCTTGATTTGCCAACAG), mouse_*Rab9* (forward: ATGGCAGGAAAATCGTCTCTTT; reverse: GCATGGTAACAAAATGTCCGTCC), mouse_*Irf7* (forward: TTTGGAGAGTGGCTATTGGGG; reverse: CCTACGA CCGAAATGCTTCCA), mouse_*Oasl1* (forward: CATGCTCCCA AGCTTCTCTCT; reverse: CTGCCATGGCTCCTCCTTTTT), and mouse_*Ifnb1* (forward: AACTCCACCAGCAGACAGTG; reverse: AGTGGAGAGCAGTTGAGGAC).

Statistical analysis

Data were shown as means ± SD; please refer to figure legends for detailed description. Data were plotted and analyzed with GraphPad Prism 9.0 software (GraphPad Software). Statistical significance was determined using one- or two-way analysis of variance (ANOVA) followed by the Sidak's multiple comparisons test. The thresholds for significance were denoted as asterisks: $^{*}P < 0.05$, $^{**}P < 0.01$, and $^{***}P < 0.001$; n.s., not significant.

Supplementary Materials

This PDF file includes:
Figs. S1 to S5
Legends for tables S1 to S3

Other Supplementary Material for this manuscript includes the following:
Tables S1 to S3

View/request a protocol for this paper from *Bio-protocol*.

REFERENCES AND NOTES

1. H. Shimura, N. Hattori, S. I. Kubo, Y. Mizuno, S. Asakawa, S. Minoshima, N. Shimizu, K. Iwai, T. Chiba, K. Tanaka, T. Suzuki, Familial Parkinson disease gene product, parkin, is a ubiquitin-protein ligase. *Nat. Genet.* **25**, 302–305 (2000).
2. D. Narendra, A. Tanaka, D. F. Suen, R. J. Youle, Parkin is recruited selectively to impaired mitochondria and promotes their autophagy. *J. Cell Biol.* **183**, 795–803 (2008).
3. S. Pickles, P. Vigie, R. J. Youle, Mitophagy and quality control mechanisms in mitochondrial maintenance. *Curr. Biol.* **28**, R170–R185 (2018).
4. S. M. Jin, M. Lazarou, C. Wang, L. A. Kane, D. P. Narendra, R. J. Youle, Mitochondrial membrane potential regulates PINK1 import and proteolytic destabilization by PARL. *J. Cell Biol.* **191**, 933–942 (2010).
5. K. Yamano, R. J. Youle, PINK1 is degraded through the N-end rule pathway. *Autophagy* **9**, 1758–1769 (2013).
6. D. P. Narendra, S. M. Jin, A. Tanaka, D. F. Suen, C. A. Gautier, J. Shen, M. R. Cookson, R. J. Youle, PINK1 is selectively stabilized on impaired mitochondria to activate Parkin. *PLOS Biol.* **8**, e1000298 (2010).
7. M. Lazarou, S. M. Jin, L. A. Kane, R. J. Youle, Role of PINK1 binding to the TOM complex and alternate intracellular membranes in recruitment and activation of the E3 ligase Parkin. *Dev. Cell* **22**, 320–333 (2012).
8. K. N. Swatek, J. L. Usher, A. F. Kueck, C. Gladkova, T. E. T. Mevissen, J. N. Pruneda, T. Skern, D. Komander, Insights into ubiquitin chain architecture using Ub-clipping. *Nature* **572**, 533–537 (2019).
9. C. Gladkova, S. L. Maslen, J. M. Skehel, D. Komander, Mechanism of parkin activation by PINK1. *Nature* **559**, 410–414 (2018).
10. A. Rakovic, J. Ziegler, C. U. Mårtensson, J. Prasuhn, K. Shurkewitsch, P. König, H. L. Paulson, C. Klein, PINK1-dependent mitophagy is driven by the UPS and can occur independently of LC3 conversion. *Cell Death Differ.* **26**, 1428–1441 (2019).
11. A. Tanaka, M. M. Cleland, S. Xu, D. P. Narendra, D. F. Suen, M. Karbowski, R. J. Youle, Proteasome and p97 mediate mitophagy and degradation of mitofusins induced by Parkin. *J. Cell Biol.* **191**, 1367–1380 (2010).
12. N. C. Chan, A. M. Salazar, A. H. Pham, M. J. Sweredoski, N. J. Kolawa, R. L. J. Graham, S. Hess, D. C. Chan, Broad activation of the ubiquitin-proteasome system by Parkin is critical for mitophagy. *Hum. Mol. Genet.* **20**, 1726–1737 (2011).
13. S. R. Yoshii, C. Kishi, N. Ishihara, N. Mizushima, Parkin mediates proteasome-dependent protein degradation and rupture of the outer mitochondrial membrane. *J. Biol. Chem.* **286**, 19630–19640 (2011).
14. M. Lazarou, D. A. Sliter, L. A. Kane, S. A. Sarraf, C. Wang, J. L. Burman, D. P. Sideris, A. I. Fogel, R. J. Youle, The ubiquitin kinase PINK1 recruits autophagy receptors to induce mitophagy. *Nature* **524**, 309–314 (2015).
15. T. Kitada, S. Asakawa, N. Hattori, H. Matsumine, Y. Yamamura, S. Minoshima, M. Yokochi, Y. Mizuno, N. Shimizu, Mutations in the parkin gene cause autosomal recessive juvenile parkinsonism. *Nature* **392**, 605–608 (1998).
16. E. M. Valente, P. M. Abou-Sleiman, V. Caputo, M. M. K. Muqit, K. Harvey, S. Gispert, Z. Ali, D. del Turco, A. R. Bentivoglio, D. G. Healy, A. Albanese, R. Nussbaum, R. González-Maldonado, T. Deller, S. Salvi, P. Cortelli, W. P. Gilks, D. S. Latchman, R. J. Harvey, B. Dallapiccola, G. Auburger, N. W. Wood, Hereditary early-onset Parkinson's disease caused by mutations in PINK1. *Science* **304**, 1158–1160 (2004).
17. I. E. Clark, M. W. Dodson, C. Jiang, J. H. Cao, J. R. Huh, J. H. Seol, S. J. Yoo, B. A. Hay, M. Guo, Drosophila pink1 is required for mitochondrial function and interacts genetically with parkin. *Nature* **441**, 1162–1166 (2006).
18. J. Park, S. B. Lee, S. Lee, Y. Kim, S. Song, S. Kim, E. Bae, J. Kim, M. Shong, J. M. Kim, J. Chung, Mitochondrial dysfunction in Drosophila PINK1 mutants is complemented by parkin. *Nature* **441**, 1157–1161 (2006).
19. S. Kawajiri, S. Saiki, S. Sato, F. Sato, T. Hatano, H. Eguchi, N. Hattori, PINK1 is recruited to mitochondria with parkin and associates with LC3 in mitophagy. *FEBS Lett.* **584**, 1073–1079 (2010).
20. C. Vives-Bauza, C. Zhou, Y. Huang, M. Cui, R. L. A. de Vries, J. Kim, J. May, M. A. Tocilescu, W. Liu, H. S. Ko, J. Magrané, D. J. Moore, V. L. Dawson, R. Grailhe, T. M. Dawson, C. Li, K. Tieu, S. Przedborski, PINK1-dependent recruitment of Parkin to mitochondria in mitophagy. *Proc. Natl. Acad. Sci. U.S.A.* **107**, 378–383 (2010).
21. J. P. Bernardini, M. Lazarou, G. Dewson, Parkin and mitophagy in cancer. *Oncogene* **36**, 1315–1327 (2017).
22. D. Hanahan, Hallmarks of cancer: New dimensions. *Cancer Discov.* **12**, 31–46 (2022).
23. C. Zhang, S. Lee, Y. Peng, E. Bunker, E. Giaime, J. Shen, Z. Zhou, X. Liu, PINK1 triggers autocatalytic activation of Parkin to specify cell fate decisions. *Curr. Biol.* **24**, 1854–1865 (2014).
24. R. G. Carroll, E. Hollville, S. J. Martin, Parkin sensitizes toward apoptosis induced by mitochondrial depolarization through promoting degradation of Mcl-1. *Cell Rep.* **9**, 1538–1553 (2014).
25. S. J. Ham, D. Lee, H. Yoo, K. Jun, H. Shin, J. Chung, Decision between mitophagy and apoptosis by Parkin via VDAC1 ubiquitination. *Proc. Natl. Acad. Sci. U.S.A.* **117**, 4281–4291 (2020).
26. J. R. Liang, A. Martinez, J. D. Lane, U. Mayor, M. J. Clague, S. Urbé, USP30 deubiquitylates mitochondrial Parkin substrates and restricts apoptotic cell death. *EMBO Rep.* **16**, 618–627 (2015).

27. S. Shimizu, T. Kanaseki, N. Mizushima, T. Mizuta, S. Arakawa-Kobayashi, C. B. Thompson, Y. Tsujimoto, Role of Bcl-2 family proteins in a non-apoptotic programmed cell death dependent on autophagy genes. *Nat. Cell Biol.* **6**, 1221–1228 (2004).
28. L. Yu, A. Alva, H. Su, P. Dutt, E. Freundt, S. Welsh, E. H. Baehrecke, M. J. Lenardo, Regulation of an ATG7-beclin 1 program of autophagic cell death by caspase-8. *Science* **304**, 1500–1502 (2004).
29. G. Kroemer, B. Levine, Autophagic cell death: The story of a misnomer. *Nat. Rev. Mol. Cell Biol.* **9**, 1004–1010 (2008).
30. D. Narendra, A. Tanaka, D. F. Suen, R. J. Youle, Parkin-induced mitophagy in the pathogenesis of Parkinson disease. *Autophagy* **5**, 706–708 (2009).
31. P. Li, D. Nijhawan, I. Budihardjo, S. M. Srinivasula, M. Ahmad, E. S. Alnemri, X. Wang, Cytochrome c and dATP-dependent formation of Apaf-1/caspase-9 complex initiates an apoptotic protease cascade. *Cell* **91**, 479–489 (1997).
32. L. Lartigue, Y. Kushnareva, Y. Seong, H. Lin, B. Faustin, D. D. Newmeyer, Caspase-independent mitochondrial cell death results from loss of respiration, not cytotoxic protein release. *Mol. Biol. Cell* **20**, 4871–4884 (2009).
33. D. R. Green, F. Llambi, Cell death signaling. *Cold Spring Harb. Perspect. Biol.* **7**, a006080 (2015).
34. S. Heimer, G. Knoll, K. Schulze-Osthoff, M. Ehrenschwender, Raptinal bypasses BAX, BAK, and BOK for mitochondrial outer membrane permeabilization and intrinsic apoptosis. *Cell Death Dis.* **10**, 556 (2019).
35. C. V. Garcia, C. S. Paim, M. Steppe, E. E. Schapoval, Development and validation of a dissolution test for rabeprazole sodium in coated tablets. *J. Pharm. Biomed. Anal.* **41**, 833–837 (2006).
36. Y. Inai, M. Yabuki, T. Kanno, J. Akiyama, T. Yasuda, K. Utsumi, Valinomycin induces apoptosis of ascites hepatoma cells (AH-130) in relation to mitochondrial membrane potential. *Cell Struct. Funct.* **22**, 555–563 (1997).
37. I. J. Furlong, C. L. Mediavilla, R. Ascaso, A. L. Rivas, M. K. Collins, Induction of apoptosis by valinomycin: Mitochondrial permeability transition causes intracellular acidification. *Cell Death Differ.* **5**, 214–221 (1998).
38. S. S. Daoud, R. L. Juliano, Reduced toxicity and enhanced antitumor effects in mice of the ionophoric drug valinomycin when incorporated in liposomes. *Cancer Res.* **46**, 5518–5523 (1986).
39. B. San Francisco, E. C. Bretsnyder, R. G. Kranz, Human mitochondrial holocytochrome c synthase's heme binding, maturation determinants, and complex formation with cytochrome c. *Proc. Natl. Acad. Sci. U.S.A.* **110**, E788–E797 (2013).
40. T. Fernandes-Alnemri, G. Litwack, E. S. Alnemri, CPP32, a novel human apoptotic protein with homology to Caenorhabditis elegans cell death protein Ced-3 and mammalian interleukin-1 beta-converting enzyme. *J. Biol. Chem.* **269**, 30761–30764 (1994).
41. F. Wauters, T. Cornelissen, D. Imberechts, S. Martin, B. Koentjoro, C. Sue, P. Vangheluwe, W. Vandenberghe, LRRK2 mutations impair depolarization-induced mitophagy through inhibition of mitochondrial accumulation of RAB10. *Autophagy* **16**, 203–222 (2020).
42. K. M. Chung, E. J. Jeong, H. Park, H. K. An, S. W. Yu, Mediation of autophagic cell death by type 3 ryanodine receptor (RyR3) in adult hippocampal neural stem cells. *Front. Cell. Neurosci.* **10**, 116 (2016).
43. D. Tapia, T. Jiménez, C. Zamora, J. Espinoza, R. Rizzo, A. González-Cárdenas, D. Fuentes, S. Hernández, V. A. Cavieres, A. Soza, F. Guzmán, G. Arriagada, M. I. Yuseff, G. A. Mardones, P. V. Burgos, A. Luini, A. González, J. Cancino, KDEL receptor regulates secretion by lysosome relocation- and autophagy-dependent modulation of lipid-droplet turnover. *Nat. Commun.* **10**, 735 (2019).
44. M. Terenzio, A. di Pizio, I. Rishal, L. Marvaldi, P. di Matteo, R. Kawaguchi, G. Coppola, G. Schiavo, E. M. C. Fisher, M. Fainzilber, DYNLRB1 is essential for dynein mediated transport and neuronal survival. *Neurobiol. Dis.* **140**, 104816 (2020).
45. F. Ning, H. Xin, J. Liu, C. Lv, X. Xu, M. Wang, Y. Wang, W. Zhang, X. Zhang, Structure and function of USP5: Insight into physiological and pathophysiological roles. *Pharmacol. Res.* **157**, 104557 (2020).
46. H. Katayama, T. Kogure, N. Mizushima, T. Yoshimori, A. Miyawaki, A sensitive and quantitative technique for detecting autophagic events based on lysosomal delivery. *Chem. Biol.* **18**, 1042–1052 (2011).
47. H. Wang, H. Meng, X. Li, K. Zhu, K. Dong, A. K. Mookhtiar, H. Wei, Y. Li, S. C. Sun, J. Yuan, PELI1 functions as a dual modulator of necroptosis and apoptosis by regulating ubiquitination of RIPK1 and mRNA levels of c-FLIP. *Proc. Natl. Acad. Sci. U.S.A.* **114**, 11944–11949 (2017).
48. A. Huett, R. J. Heath, J. Begun, S. O. Sassi, L. A. Baxt, J. M. Vyas, M. B. Goldberg, R. J. Xavier, The LRR and RING domain protein LRSAM1 is an E3 ligase crucial for ubiquitin-dependent autophagy of intracellular Salmonella Typhimurium. *Cell Host Microbe* **12**, 778–790 (2012).
49. Y. Feng, B. Press, A. Wandinger-Ness, Rab 7: An important regulator of late endocytic membrane traffic. *J. Cell Biol.* **131**, 1435–1452 (1995).
50. K. Yamano, C. Wang, S. A. Sarraf, C. Münch, R. Kikuchi, N. N. Noda, Y. Hizukuri, M. T. Kanemaki, W. Harper, K. Tanaka, N. Matsuda, R. J. Youle, Endosomal Rab cycles regulate Parkin-mediated mitophagy. *eLife* **7**, e31326 (2018).
51. T. Saito, J. Nah, S. I. Oka, R. Mukai, Y. Monden, Y. Maejima, Y. Ikeda, S. Sciarretta, T. Liu, H. Li, E. Baljinnyam, D. Fraidenraich, L. Fritzky, P. Zhai, S. Ichinose, M. Isobe, C. P. Hsu, M. Kundu, J. Sadoshima, An alternative mitophagy pathway mediated by Rab9 protects the heart against ischemia. *J. Clin. Invest.* **129**, 802–819 (2019).
52. R. L. Deter, P. Baudhuin, C. De Duve, Participation of lysosomes in cellular autophagy induced in rat liver by glucagon. *J. Cell Biol.* **35**, C11–C16 (1967).
53. V. Rogov, V. Dotsch, T. Johansen, V. Kirkin, Interactions between autophagy receptors and ubiquitin-like proteins form the molecular basis for selective autophagy. *Mol. Cell* **53**, 167–178 (2014).
54. T. N. Nguyen, B. S. Padman, J. Usher, V. Oorschot, G. Ramm, M. Lazarou, Atg8 family LC3/GABARAP proteins are crucial for autophagosome-lysosome fusion but not autophagosome formation during PINK1/Parkin mitophagy and starvation. *J. Cell Biol.* **215**, 857–874 (2016).
55. J. M. Heo, A. Ordureau, J. A. Paulo, J. Rinehart, J. W. Harper, The PINK1-PARKIN mitochondrial ubiquitylation pathway drives a program of OPTN/NDP52 recruitment and TBK1 activation to promote mitophagy. *Mol. Cell* **60**, 7–20 (2015).
56. B. Richter, D. A. Sliter, L. Herhaus, A. Stolz, C. Wang, P. Beli, G. Zaffagnini, P. Wild, S. Martens, S. A. Wagner, R. J. Youle, I. Dikic, Phosphorylation of OPTN by TBK1 enhances its binding to Ub chains and promotes selective autophagy of damaged mitochondria. *Proc. Natl. Acad. Sci. U.S.A.* **113**, 4039–4044 (2016).
57. H. Kalkavan, M. J. Chen, J. C. Crawford, G. Quarato, P. Fitzgerald, S. W. G. Tait, C. R. Goding, D. R. Green, Sublethal cytochrome c release generates drug-tolerant persister cells. *Cell* **185**, 3356–3374.e22 (2022).
58. M. J. White, K. McArthur, D. Metcalf, R. M. Lane, J. C. Cambier, M. J. Herold, M. F. van Delft, S. Bedoui, G. Lessene, M. E. Ritchie, D. C. S. Huang, B. T. Kile, Apoptotic caspases suppress mtDNA-induced STING-mediated type I IFN production. *Cell* **159**, 1549–1562 (2014).
59. A. Rongvaux, R. Jackson, C. C. D. Harman, T. Li, A. P. West, M. R. de Zoete, Y. Wu, B. Yordy, S. A. Lakhani, C. Y. Kuan, T. Taniguchi, G. S. Shadel, Z. J. Chen, A. Iwasaki, R. A. Flavell, Apoptotic caspases prevent the induction of type I interferons by mitochondrial DNA. *Cell* **159**, 1563–1577 (2014).
60. B. C. Hammerling, R. H. Najor, M. Q. Cortez, S. E. Shires, L. J. Leon, E. R. Gonzalez, D. Boassa, S. Phan, A. Thor, R. E. Jimenez, H. Li, R. N. Kitsis, G. W. Dorn II, J. Sadoshima, M. H. Ellisman, Å. B. Gustafsson, A Rab5 endosomal pathway mediates Parkin-dependent mitochondrial clearance. *Nat. Commun.* **8**, 14050 (2017).
61. Y. Qiu, J. Wang, H. Li, B. Yang, J. Wang, Q. He, Q. Weng, Emerging views of OPTN (optineurin) function in the autophagic process associated with disease. *Autophagy* **18**, 73–85 (2022).
62. S. Zhang, Z. Shao, X. Liu, M. Hou, F. Cheng, D. Lei, H. Yuan, The E50K optineurin mutation impacts autophagy-mediated degradation of TDP-43 and leads to RGC apoptosis in vivo and in vitro. *Cell Death Discov.* **7**, 49 (2021).
63. J. M. Heo, A. Ordureau, S. Swarup, J. A. Paulo, K. Shen, D. M. Sabatini, J. W. Harper, RAB7A phosphorylation by TBK1 promotes mitophagy via the PINK-PARKIN pathway. *Sci. Adv.* **4**, eaav0443 (2018).
64. C. Wang, R. J. Youle, Predominant requirement of Bax for apoptosis in HCT116 cells is determined by Mcl-1's inhibitory effect on Bak. *Oncogene* **31**, 3177–3189 (2012).
65. S. W. G. Tait, A. Oberst, G. Quarato, S. Milasta, M. Haller, R. Wang, M. Karvela, G. Ichim, N. Yatim, M. L. Albert, G. Kidd, R. Wakefield, S. Frase, S. Krautwald, A. Linkermann, D. R. Green, Widespread mitochondrial depletion via mitophagy does not compromise necroptosis. *Cell Rep.* **5**, 878–885 (2013).
66. F. Llambi, Y. M. Wang, B. Victor, M. Yang, D. M. Schneider, S. Gingras, M. J. Parsons, J. H. Zheng, S. A. Brown, S. Pelletier, T. Moldoveanu, T. Chen, D. R. Green, BOK is a non-canonical BCL-2 family effector of apoptosis regulated by ER-associated degradation. *Cell* **165**, 421–433 (2016).
67. N. E. Sanjana, O. Shalem, F. Zhang, Improved vectors and genome-wide libraries for CRISPR screening. *Nat. Methods* **11**, 783–784 (2014).
68. S. Sharma, A. Rao, RNAi screening: Tips and techniques. *Nat. Immunol.* **10**, 799–804 (2009).
69. J. H. Zhang, T. D. Chung, K. R. Oldenburg, A simple statistical parameter for use in evaluation and validation of high throughput screening assays. *J. Biomol. Screen.* **4**, 67–73 (1999).

Acknowledgments: We thank R. Youle for providing the *Bax*$^{-/-}$ *Bak*$^{-/-}$ MEFs, the WT and *Bax*$^{-/-}$ *Bak*$^{-/-}$ HCT116 cells, the OPA3-PINK1 Δ1–110 plasmid, and the pCHAC-mt-mKeima plasmid. We thank M. Lazarou for providing the HeLa cells: WT, LC3 TKO, GABARAP TKO, ATG8 6KO, and ATG-R 5KO. We thank the Hartwell Center and Y.-D. Wang from the Department of Cell and Molecular Biology at St. Jude Children's Research Hospital for the assistance with the genomes sequencing related to the CRISPR screen. We thank B. S. Hansen and S. M. Pruett-Miller from the

Center for Advanced Genomic Engineering at St. Jude Children's Research Hospital for assistance with CRISPR cell line validation. Transmission electron microscopy images were acquired at the Cell and Tissue Imaging Center at St. Jude Children's Research Hospital. G.Q. thanks F. Llambi and T. Moldoveanu for helpful discussions and advice. We thank K. Verbist and H. M. Beere for a critical review of the manuscript. Cartoons were created with BioRender.com. **Funding:** This research was supported by R35CA231620 from the U.S. National Cancer Institute. The transmission electron microscopy facility, the Hartwell Center, and the Center for Advanced Genome Engineering were supported by St. Jude Children's Research Hospital and NCI P30 CA021765. The content is solely the responsibility of the authors and does not necessarily represent the official views of the National Institutes of Health. **Author contributions:** Conceptualization: G.Q., L.M., and D.R.G. Methodology: G.Q., L.M., N.J.B., M.Y., S.R., M.J.C., C.S.G., and J.L. Investigation: G.Q., L.M., and D.R.G. Visualization: G.Q. and L.M. Supervision: T.C. and D.R.G. Writing (original draft): G.Q., L.M., and D.R.G. **Competing interests:** D.R.G. consults for Sonata Therapeutics, Horizon Therapeutics, and Ventus Therapeutics. All other authors declare that they have no competing interests. **Data and materials availability:** All data needed to evaluate the conclusions in the paper are present in the paper and/or the Supplementary Materials. The data for the CRISPR KO screen in this study have been deposited with links to BioProject PRJNA956539 in the NCBI BioProject database (www.ncbi.nlm.nih.gov/bioproject/).

Submitted 24 January 2023
Accepted 18 April 2023
Published 24 May 2023
10.1126/sciadv.adg8156